INTERNATIONAL JOURNAL OF HYDROGEN ENERGY 52 (2024) 1084–1103

Available online at www.sciencedirect.com

ScienceDirect

journal homepage: www.elsevier.com/locate/he

Optimal decarbonization strategies for an industrial port area by using hydrogen as energy carrier

Davide Pivetta [a], *Gabriele Volpato* [b], *Gianluca Carraro* [b], *Chiara Dall'Armi* [a], *Luca Da Lio* [b], *Andrea Lazzaretto* [b], *Rodolfo Taccani* [a,*]

[a] *Department of Engineering and Architecture, University of Trieste, Via Valerio 10, 34127, Trieste, Italy*
[b] *Department of Industrial Engineering, University of Padova, Via Venezia 1, 35131, Padova, Italy*

HIGHLIGHTS

- Energy/hydrogen demands of industry and port equipment/vehicles are considered.
- 32 optimization runs are performed under different cost and emission scenarios.
- Optimal set of decarbonization strategies is selected for a real industrial port area.
- Electrification/hybridization play a key role in medium/long-term decarbonization.
- Hydrogen technologies ensure a deep decarbonization of the system in 2050.

ARTICLE INFO

Article history:
Received 30 March 2023
Received in revised form
6 June 2023
Accepted 2 July 2023
Available online 14 September 2023

Keywords:
Water electrolysis
Hydrogen carrier
Industrial port area
Port decarbonization
Cargo handling equipment
Hard-to-abate industry

ABSTRACT

This article discusses possible strategies for decarbonizing the energy systems of an existing port. The approach consists in creating a complete superstructure that includes the use of renewable and fossil energy sources, the import or local production of hydrogen, vehicles and other equipment powered by Diesel, electricity or hydrogen and the associated refuelling and storage units. Two substructures are then identified, one including all these options, the other considering also the addition of the energy demand of an adjacent steel industry. The goal is to select from each of these two substructures the most cost-effective configurations for 2030 and 2050 that meet the emission targets for those years under different cost scenarios for the energy sources and conversion/storage units, obtained from the most reliable forecasts found in the literature. To this end, the minimum total cost of all the energy conversion and storage units plus the associated infrastructures is sought by setting up a Mixed Integer Linear Programming optimization problem, where integer variables handle the inclusion of the different generation and storage units and their activation in the operational phases. The comprehensive picture of possible solutions set allows identifying which options can most realistically be realized in the years to come in relation to the different assumed cost scenarios. Optimization results related to the scenario projected to 2030 indicate the key role played by Diesel hybrid and electric systems, while considering the most stringent, or much more stringent, scenarios for

Acronyms: $CO_{2,eq}$, Carbon dioxide equivalent; GH_2, Gaseous hydrogen; H_2, Hydrogen; HP, High-Pressure; HRS, Hydrogen Refuelling Station; IPA, Industrial Port Area; LH_2, Liquid hydrogen; LP, Low-Pressure; MILP, Mixed-Integer Linear Programming; NH_3, Ammonia; PEME, Proton Exchange Membrane Electrolyzer; PV, PhotoVoltaic; RES, Renewable Energy Sources; TEU, Twenty-foot Equivalent Unit; WT, Wind Turbines.

* *Corresponding author*. University of Trieste, Department of Engineering and Architecture, Via Valerio 10, Trieste, Italy.
E-mail address: taccani@units.it (R. Taccani).

https://doi.org/10.1016/j.ijhydene.2023.07.008

0360-3199/© 2023 The Authors. Published by Elsevier Ltd on behalf of Hydrogen Energy Publications LLC. This is an open access article under the CC BY license (http://creativecommons.org/licenses/by/4.0/).

emissions in 2050, almost all vehicles energy demand and industry hydrogen demand is met by hydrogen imported as ammonia by ship.

© 2023 The Authors. Published by Elsevier Ltd on behalf of Hydrogen Energy Publications LLC. This is an open access article under the CC BY license (http://creativecommons.org/licenses/by/4.0/).

Introduction

Nowadays the reduction of greenhouse gas emissions is an overriding objective to bound the global temperature increase to 1.5 °C [1]. The achievement of this goal demands for a major transition in just a few decades by acting not only on the energy sector, but also on transportation and industrial production chains. Industrial Port Areas (IPAs) are energy-demanding centres. IPAs represent central hubs that facilitate seaborne trade [2], with transport of goods and raw materials, and usually host processing industries that take advantage of the direct commodities supply and strategic position [3]. However, the operation of IPAs is responsible for large amounts of pollutant and greenhouse gas emissions (e.g., carbon dioxide (CO_2), nitrogen oxides (NO_X), sulphur oxides (SO_X), particulate matter etc.). The sources of emissions in IPAs operation can be summarized as: (i) fleets of vehicles for cargo handling and goods movement ranging from yard tractors, reach stackers, forklifts, cranes, trains, etc. [4], (ii) process industries close to the port area (e.g., chemical industries, steel production plants [3,5]), (iii) heating, ventilation and air conditioning systems of the buildings and warehouses [6], (iv) ships that keep their engines idling when they are docked to generate electricity for onboard living systems [7].

In addition, more than 90% of ports is in the proximity of city areas and therefore ports have a significant environmental impact locally, posing serious risks for the health of people living in the surrounding areas [8]. Projections to 2050 estimate that ports will generate about 70 million tons of CO_2 and 1.3 million tons of NO_X [2]. Hence, to limit the environmental and health impact of IPAs, the decarbonization of port energy systems, port fleet vehicles and industries in the surroundings is crucial. The decarbonization of such systems is a complex issue, and the main strategies to address it are:

1) electrification and automation of equipment and vehicles;
2) renewable energy systems and associated smart grids, use of alternative fuels as hydrogen (H_2) and ammonia (NH_3);
3) increase of energy efficiency of machinery and buildings;
4) cold ironing [9].

The attention here is on items 1) and 2).

Electrification and hybridization of cargo handling equipment and vehicles are attractive options to reduce local pollutant and greenhouse gases emission in the medium term [10]. In their recent review article, Cunanan et al. [11] examined the suitability of diesel, battery electric, and hybrid H_2 powertrains for heavy-duty vehicle applications. The authors provided a comprehensive comparison of these powertrains, taking into account their working mechanisms, performance metrics, and recent advancements, and highlighting their strengths and limitations. Kim et al. [12] performed a comparative life-cycle analysis of Diesel and electric yard tractors in the Port of Los Angeles (USA), establishing that the electrification of half of the yard tractor fleet could lower the emissions by up to about 60%. Hong-Lei et al. [13] demonstrated by a numeric simulation that the replacement of a traditional Diesel crane with a hybrid electric rubber-tired gantry crane results in a 70% savings of CO_2 emissions. Ilio et al. [14] designed a fuel-cell hybrid battery for a H_2-fuelled yard truck, used in cargo handling port operations, with the aim of obtaining zero local CO_2 emissions from this vehicle. Densberger and Bachkar [15] conducted a review about the decarbonization of ports with a particular emphasis on the adoption of zero-emissions cargo handling equipment in the ports of Los Angeles and Long Beach (USA).

On the other hand, several studies in the literature dealt with the use of RES and smart grids in ports, showing that they could not only improve the environmental performance of port systems but also the economic cost savings [16–18]. Ahamad et al. [16] found that RES-based smart grids could reduce the port environmental impact and 75% RES share could be achieved by using existing power and energy storage technologies in the Port of Copenhagen (DK). Wang et al. [17] addressed the design and operation optimization of microgrids in ports, by considering the exploitation of multiple RES distributed within the microgrids. Prousalidis et al. [18] proposed the creation of a smart energy system in port efficiently matching RES production with cold-ironing power demand. Geerlings et al. [19] investigated the beneficial effects of efficient scheduling of port activities to minimize peaks of the energy demands and, in turn, reduce the required generation power to be installed. Results show that by optimally scheduling the ship-to-shore crane operations, up to 50% of the peak demand can be reduced, with a consequent decrease in the total peak-related costs of about 48%. In recent years, the use of alternative fuels and energy carriers is gaining a growing interest. In particular, the so-called green H_2, i.e., H_2 generated via electrolysis powered by renewable electric energy, seems to be a promising option for decarbonization [20]. Indeed, H_2 could be used not only to decarbonize heavy-duty vehicles for cargo handling in the port [14], but also to achieve zero emission shipping [21–24] and make hard-to-abate industrial processes more environmentally friendly [20]. Furthermore, green H_2 allows to overcome the limitations of intermittent RES (e.g., solar, wind) by its storage in compressed or liquefied form [25]. Thus, IPAs could become sites of energy and H_2 production, storage and exchange, i.e., real smart energy hubs [26]. Regarding transportation, H_2 can be delivered by trucks (till 300–500 km) and ships (4000–9000 km) for short and long distances, respectively. The transportation of H_2 by ships requires its liquefaction or conversion into NH_3. Mallouppas et al. [27] highlighted that NH_3 is a promising

solution as direct or indirect H_2 carrier, and its share in the fuel mix of the maritime sector could rise from 7% in 2030 to 20–25% in 2050. As reported in Ref. [28], 45% of the traded H_2 in 2050 will be transported as NH_3 by ships, without requiring a final reconversion to H_2 in the case NH_3 is used as chemical feedstock or fuel (e.g., for the maritime and aviation sectors). In fact, shipping NH_3 is less expensive than shipping liquified H_2 (LH_2) given the higher density, the simpler conditions for storage, and the lower price of NH_3 due to the availability of already existing infrastructures. On the other hand, shipping LH_2 could be more advantageous in case of short distances of transportation by ship (for 4000 km and where pipelines are not an option) [29]. Another way to transport and use LH2 could be using innovative swapable containers as in the case of the sHYpS project, where these containers are used for ship propulsion [30].

The literature review about decarbonization strategies 1) and 2) highlights the positive environmental effects of using renewable energy in powering hybrid and electric cargo handling equipment and vehicles. Nevertheless, to the best of the authors' knowledge, no studies in the literature consider both the various powertrain options for these equipment/vehicles and the infrastructure for their optimal management. This paper deals with all these aspects in an IPA located in the Northern Italy, including the possibility of generating H_2 locally, or importing it by ship and consuming it either in the port vehicles fleet or in any adjacent industry. A "superstructure" is so created that includes all the alternative/complementary proposed solutions for the energy systems of the port, consisting in:

(i) the exploitation of solar and wind energy for electricity generation and storage;
(ii) the import of grey and green H_2 (LH_2 or NH_3 by ships, and gaseous H_2 (GH_2) by trucks), the production of and storage of green H_2, and the use of both green and grey H_2 for mobility and industrial applications;
(iii) the alternative options for mobility: Hybrid Diesel, electric and H_2 fuelled vehicles, integrated with all their refuelling/charging stations and infrastructures.

The goal is to "extract" from the superstructure the most cost-effective configuration of the port energy systems for different possible levels of carbon dioxide equivalent ($CO_{2,eq}$) emissions that might be imposed by environmental regulations. These emissions are calculated by considering the global warming potential over 100 years of gases emitted directly or indirectly from the use of energy sources.

The optimal configuration in terms of cost comprises:

a. the design and operation of the energy conversion and storage units that fulfil the energy and H_2 demands of the port vehicles and any possible H_2 demand of the nearby steel industry.
b. the set of powertrains of the port fleet vehicles.
c. the amount of imported H_2 as LH_2 or NH_3.

A Mixed Integer Linear Programming (MILP) design-operation optimization problem is set up based on one-year operation of the port. The problem is solved considering two main substructures: one including the energy demand of both industry and port vehicles/equipment, the other one including only the energy demand of port vehicles/equipment.

For both substructures, the total capital and operating costs of the IPA's energy conversion and storage systems with related infrastructure, are minimized for different scenarios of emission targets and costs in 2030 and 2050. The projected values in those years for the costs of all energy conversion and storage units and infrastructure, and for the prices of imported H_2 are used as input values. The possible deviations in the costs of electric vehicles and charging stations from those projected are considered to account for additional market uncertainties.

The total thirty-two optimization runs aim at providing a comprehensive picture of the possible evolution of the energy conversion and storage systems configurations in the IPA, still not existing in the present literature.

Energy system description

The Port of Trieste, an Italian port located in North-Adriatic Sea, is here considered as a case study. This work analyses the real number of port cargo handling equipment and vehicles operating in the considered port, which is representative of a medium-size container port with a yearly cargo capacity of about 1 million TEU (Twenty-foot Equivalent Unit). Yearly fuel demand and characteristics of port cargo handling equipment and vehicles fleet are estimated from data collected in Ref. [6]. The Industrial Port Area (IPA) under analysis evaluates two energy demands, i.e., the energy demand of the port equipment and vehicles and the H_2 demand of an industry operating in the port area. This study does not consider other energy requirements such as those for buildings, warehouses, lighting systems, and cold ironing infrastructure. While power demand of buildings, warehouses, and lighting systems has a low impact on the total emissions of the port, the use of cold ironing, which involves supplying electrical power to ships while they are docked, has the potential to significantly reduce emissions in ports. However, implementing cold ironing can be expensive and requires a substantial increase in the grid capacity of the port [31]. In situations where the national power grid cannot meet the demand for cold ironing, new renewable power plants should be built locally. Photovoltaic and hydrogen-to-power solutions may be viable options, but their implementation is usually limited by factors such as the available surface area for installation and the high cost of stationary fuel cells. These limitations and uncertainties make cold ironing a decarbonization strategy that is not among the first to be easily implemented and, as such, is not considered in this paper.

In this Section, the existing and the new energy conversion and storage units are listed and the analytical relationships describing the energy flow entering and outgoing from each unit are introduced.

The schematic of Fig. 1 shows the layout of the energy system. Arrows of different colour identify the flows of H_2 (blue lines), electric power (green lines), solar/wind power (yellow lines) and Diesel (black lines). Dashed lines mark the whole system boundaries (black dashed lines), the H_2/energy

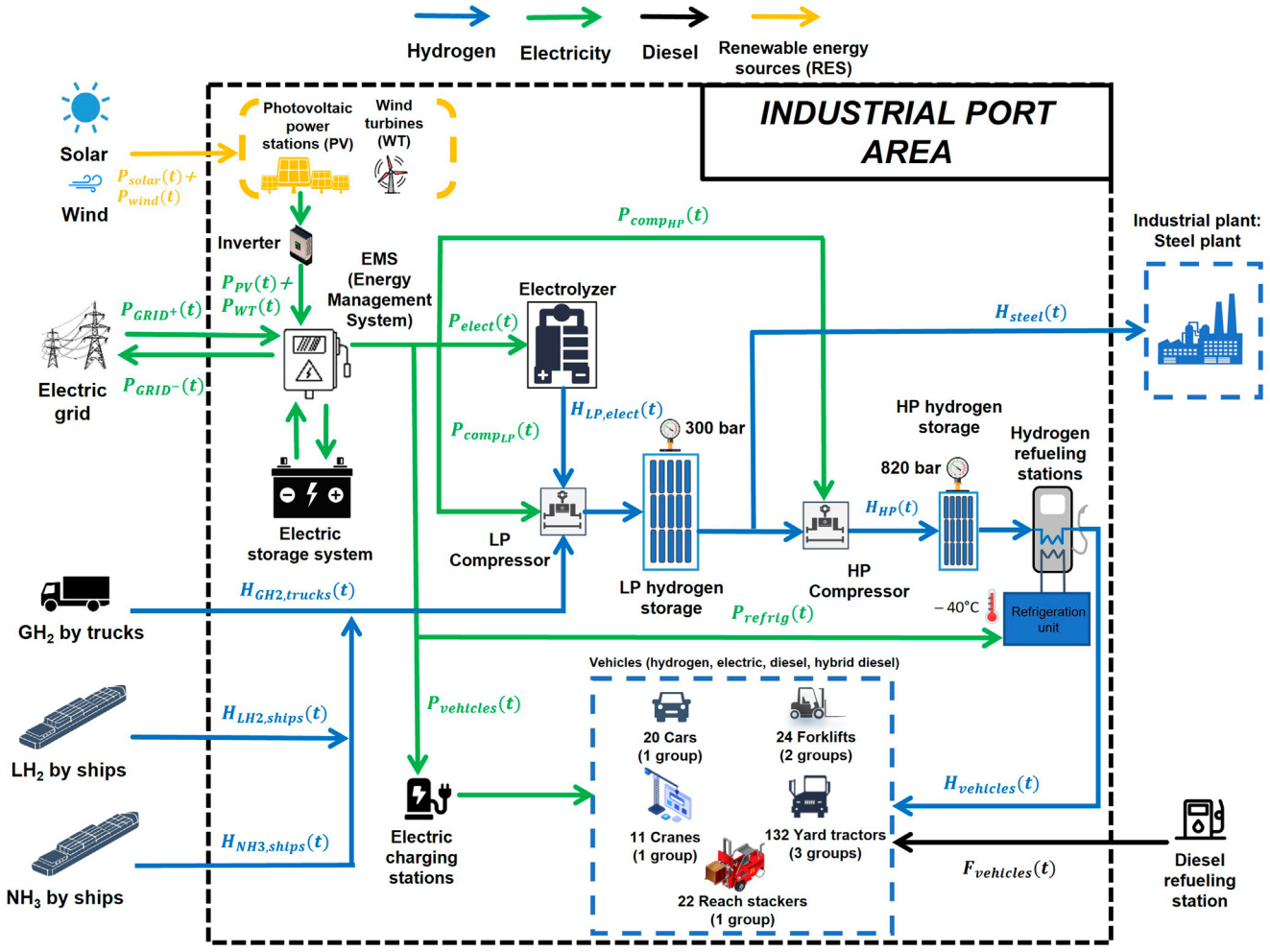

Fig. 1 – Layout of the IPA energy system. Arrows identify the flows of H_2 (blue), electric power (green), solar/wind power (yellow) and Diesel (black). Dashed lines are the boundaries of the whole system optimization model (black), available renewable energy sources (yellow) and H_2/energy user units (blue). (For interpretation of the references to colour in this figure legend, the reader is referred to the Web version of this article.)

user units (blue dashed lines) and the available renewable energy sources (yellow dashed lines).

Starting from the upper left side of Fig. 1, solar and wind energy available at the selected location could be exploited by the PhotoVoltaic (PV) power plant and Wind Turbines (WT), respectively. Electric power from RES and/or purchased from the electric grid is directed to the energy management system that, in turn, dispatches the power either outwards the electric grid or inwards the stationary Li-ion electric storage system, and/or port electric users. These are the electric charging stations for the electric vehicle fleet, the Proton Exchange Membrane Electrolyzer (PEME) for H_2 local production by water electrolysis, the H_2 compression station at two pressure levels equipped with two-stage reciprocating compressors, and the Hydrogen Refuelling Station (HRS) for the vehicles and equipment fleet.

The HRS includes a dispenser (its electric consumption is neglected) and a refrigeration unit that cools the H_2 during the operations of vehicle tank refuelling. The cooling ensures the full filling of the on-board vehicle tanks and avoids safety hazards (referring to the standard SAE-J2601 [32]).

As for PEME, neither the water consumption, nor the utilisation of oxygen produced via water electrolysis are accounted in the cost analysis because of the low cost of water [33], the low price of oxygen for industrial use and the absence of a mature market for oxygen produced from RES [34]. H_2 could be also imported via truck in gaseous form (GH_2), or via ship in liquid form as LH_2 or NH_3. The cost and carbon impact of imported H_2 include the production, fuel-processing, and transport.

Two energy demands (circled by blue dashed lines) are considered: the energy demand of the port vehicles and equipment, consisting in cars, forklifts, cranes, yard tractors and reach stackers, and the hydrogen demand of a steel industry operating in the port area. The former could be supplied by a combination of Diesel, electricity and/or hydrogen, depending on the type of powertrain chosen for each type of equipment and vehicles, as detailed in Section Modelling and optimization.

In the following, Section Energy inputs introduces the external energy inputs of the IPA. Section Energy and hydrogen demands presents the H_2/energy demands.

Definition of energy and market scenarios illustrates the four future energy scenarios simulated in the analysis differing in $CO_{2,eq}$ emission reduction, cost of H_2 imported and cost of electric equipment and vehicles.

Energy inputs

The external inputs to the IPA are the electricity from the grid, the H_2 import, the RES exploited (i.e., wind and solar energy) and the import of Diesel oil. A more detailed description of these energy inputs follows:

Electricity
The IPA can purchase and sell electricity from and to the national power grid. The power capacity of national power grid is assumed to be infinite both for the import and export, and power losses due to the power transfer to/from the port internal grid are neglected. The carbon footprint of the power purchased from the national grid is evaluated at hourly basis according to the Italian market scenario in 2019 [35]. It spans a range between 141 and 475 $gCO_{2,eq}$/kWh due to variation of the power production mix in Italy and the import/export of power. The electricity purchase prices in 2030 and 2050 are estimated to be about 7 and 8 c€/kWh, while the selling price of power produced by local RES is estimated to be about 6 c€/kWh in both 2030 and 2050 [36].

Hydrogen import sources
It is assumed that H_2 could be delivered to the port via trucks or ships. Three external H_2 supply sources are considered: Gaseous Hydrogen (GH_2) imported via trucks, Liquid Hydrogen (LH_2) via ships and liquid ammonia (NH_3) via ships. It is assumed that GH_2 is produced by steam methane reforming with a fixed cost of about 2 €/kg_{H2} and transported for a relatively short distance (~500 km), corresponding to a carbon footprint of about 10 $kg_{CO2,eq}/kg_{H2}$ [37]. As for the import of LH_2 and NH_3 via ships, a prediction of cost and carbon footprint (expressed as $kg_{CO2,eq}$ per kg of H_2) in 2030 and 2050 is provided from data available in the literature, as detailed in the Supplementary Material.

The imported H_2 enters the control system at 30 bar, is compressed up to 300 bar by the Low-Pressure (LP) compressor and then stored in the LP tank. The 300 bar pressure level is a good compromise between cost and volume of the vessel and allows the direct transfer of H_2 towards the steel plant. Instead, the H_2 for the port equipment and vehicles requires a further compression up to 820 bar and is stored in the proximity of the refuelling stations. This pressure level guarantees the refuelling of on-board vehicle tanks to a maximum pressure of about 700 bar by the only pressure difference.

Renewable energy sources
A solar PV power plant and/or WTs provide renewable-based energy. The size of these plants is consistent with the available surface in the port of Trieste, i.e., the PV is limited to 20 MW of peak power and the maximum number of WTs is 10.

Diesel
The input of Diesel oil powers the fleet of Diesel/hybrid Diesel equipment and vehicles (i.e., cars, forklifts, reach stackers, cranes and yard tractors). Both the capital and operating and maintenance costs of Diesel refuelling stations are neglected, being considerably lower than the other equipment (a H_2 refuelling system is about ten times more expensive) [38].

Energy and hydrogen demands

This Section deals with the energy demand of the IPA, i.e., the hydrogen demand of a steel industry located in the vicinity of the port and the energy demand of the cargo handling equipment and vehicles operating in the Port of Trieste. These demands are modelled as hourly profiles over a year and represent input parameters for the optimization model.

Hydrogen demand of steel industry
Iron and steel industries are responsible for approximately 7–9% of the total global greenhouse gas emissions [39]. Currently, around three-quarters of steel production relies on coal, whereas the remainder comes from the recycling of existing steel using electric arc furnaces. Despite improvements in steel production processes, 0.77 tons of coal per ton of new steel are still required. Compared to the coal-based steel production processes, the use of H_2 allows a remarkable increase in the energy efficiency of the process. Consequently, the industry sector is exploring the use of H_2 as an alternative energy source to reduce the environmental impact [39–41]. Full-scale experiments using pure H_2 are already underway at the SSAB steelworks in Sweden. It is estimated that a ton of finished new steel would require only 3 MWh (about 90 kg of H_2) instead of the 6 MWh of coal-based production processes [42]. Despite the transitioning to H_2 production from RES via electrolysis or biomass-based processes is costly [39], it can revolutionize the iron and steel industry and significantly reduce its impact on the environment.

In this study, a cold rolling plant for steel refining is considered. It represents a typical case of the so-called hard-to-abate industry, where the H_2 is used as feedstock for the annealing process in bell furnaces. The plant requires a steady H_2 flow of 1000 t/y at about 10 bar [42–44]. The analysis in this work evaluates the total or partial replacement of the grey hydrogen currently used with that either imported (via ship or via truck) or locally produced in the port by RES. The production cost of the grey hydrogen (considering the production via steam methane reforming) is 2 €/kgH_2 while the carbon footprint is 10 $kgCO_{2,eq}/kgH_2$.

Energy demands of port equipment and vehicles (hydrogen, electricity and Diesel)
The *equipment and vehicle types* (denoted as *v* in Section Energy and mass balances of the total system and Section Powertrain options for port equipment and vehicles) operating in the port are cars, forklifts, cranes, yard tractors and reach stackers. In the baseline scenario, all equipment and vehicles are powered by Diesel engines. The daily net mechanical energy required by each unit is estimated starting from the Diesel annual consumption and assuming a continuous operation during the year with a typical Diesel engine efficiency. All *equipment and vehicle types* include several units that are divided into different *groups* and are powered by four possible *powertrains*

Table 1 – Number of equipment and vehicles, number of groups, and daily unit energy/fuel demands of each equipment and vehicle type (rows) and powertrains (columns).

	Number of Equip&veh (–)	Number of groups (*gp*) (–)	Diesel (l_{Diesel}/day)	Hybrid Diesel (l_{Diesel}/day)	Hybrid hydrogen (kg_{H2}/day)	Electric energy (kWh/day)
Car	20	1	4.0	2.8	0.6	5
Forklift	24	2	35.4	24.8	5.0	41
Crane	11	1	318.2	222.8	45.0	677
Yard tractor	132	3	148.5	103.9	21.0	173
Reach stacker	22	1	176.8	106.1	25.0	165

(named "pt"), i.e., hybrid-hydrogen (i.e., electric motor fed by a hydrogen fuelled fuel cell or by a battery, pt = 1), full electric (i.e., electric motor fed by a battery, pt = 2), Diesel (i.e., internal combustion engine, pt = 3) and hybrid-Diesel (i.e., electric motor fed by Diesel internal combustion engine or by a battery, pt = 4). Note that only the full electric powertrain is a plug-in solution that absorbs electric power from an external source; in the other powertrain options the electric energy is produced on board from the fuel (Diesel or hydrogen). The conversion efficiency of the powertrain allows calculating the energy input in terms of the corresponding fuel (daily Diesel mass and hydrogen mass), while the electrical demand is assessed on the basis of the performance and characteristics of existing equipment and vehicles of the different types (cars [45], forklifts [46], cranes [47], tractors [48,49], and reach stackers [49,50]).

The choice of the powertrain for the whole car fleet is treated as a single variable in the optimization model (see Section Powertrain options for port equipment and vehicles), i.e., all cars might have Diesel, or hybrid Diesel, or hybrid hydrogen or full electric powertrains. The simultaneous presence of two or more powertrains in the car fleet is not allowed. In this sense, cars represent at most only one *group* (index gp), i.e., they share a common *powertrain*. The same model architecture is valid for cranes and reach stackers. Conversely, forklift and yard tractors fleets are divided into two and three equinumerous groups, respectively, due to their higher number. The presence of more than one *group* for an *equipment and vehicle type* means that different powertrains can be selected for those vehicles (one powertrain for each group). This choice is a good trade-off between computational effort and accuracy in assessing the cost and performance of electric equipment and vehicle charging infrastructure and hydrogen equipment and vehicle refuelling stations. Table 1 reports the number of vehicles, the number of *groups* and the daily energy/fuel demands of each *equipment and vehicle type* (rows) and *powertrain* (columns) combination. Section Powertrain options for port equipment and vehicles reports the mathematical formulation that allows the optimizer to choose the optimal *powertrain* for each *group* of *equipment and vehicle type*.

It is assumed that each equipment and vehicle is refuelled or charged once per day, based on a specific schedule that has been evaluated for each group of equipment and vehicles. This charging/refuelling schedule ensures that each equipment and vehicle has enough energy to operate throughout the day. Fig. 2 shows as an example the typical daily charging/refuelling schedule of a group of forklifts. Blue dotted line

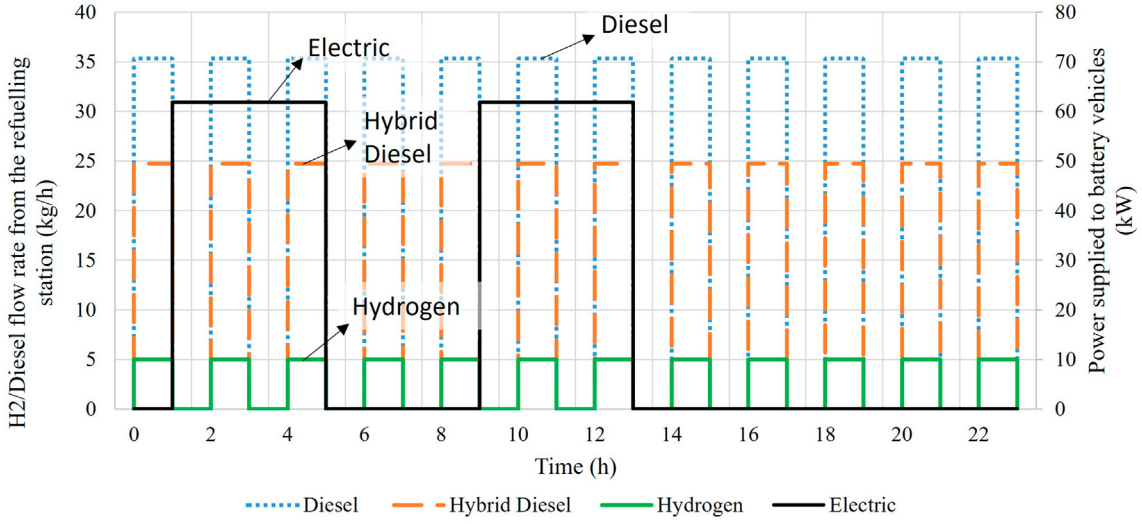

Fig. 2 – Typical daily charging/refuelling schedule of a single group of forklifts. Blue dotted line (Diesel, left axis) represents the Diesel refuelled to the Diesel forklifts over the working day, orange dashed line (Hybrid Diesel, left axis) the Diesel refuelled to hybrid Diesel forklifts, green line (Hydrogen, left axis) the hydrogen refuelled to hybrid hydrogen forklifts. Black line (electric, right axis) represents the power supplied by the electric charging station to the battery electric forklifts. (For interpretation of the references to colour in this figure legend, the reader is referred to the Web version of this article.)

(*Diesel, left axis*) represents the Diesel refuelled to the Diesel forklifts over the working day, orange dashed line (*Hybrid Diesel, left axis*) the Diesel refuelled to hybrid Diesel forklifts, green line (*Hydrogen, left axis*) the hydrogen refuelled to hybrid hydrogen forklifts. Black line (*electric, right axis*) represents the power supplied by the electric charging station to the battery electric forklifts. The integrals of the curves in Fig. 2 are the daily consumptions of one forklift group, in accordance with data in Table 1.

Differently from the Diesel refuelling stations, the cost of electric charging stations for full-electric powertrains is considered in the optimization model. Electric charging stations are designed to recharge the battery bank within approximately 2 h to prevent degradation due to a too rapid recharge [51]. An electric charging station with one or more charging connectors is sized according to the number of equipment and vehicles and the power capacity, and its technical and economic characteristics are obtained from commercial technologies [52–54] and costs are reported in the Supplementary Material. In the example of Fig. 2, for a group of forklifts (12 vehicles), daily charging schedule is defined to charge three forklifts simultaneously, six in the morning and six in the afternoon, in order to maintain continuity of service.

Equipment and vehicles equipped with hybrid hydrogen powertrains require Hydrogen Refuelling Stations (HRSs) that cool down the hydrogen to −40 °C to avoid underfilling of onboard tanks according to the standard SAE-J2601 [32]. Two types of HRSs are considered: those for the refuelling of cars and forklifts with a dispensing capacity of 100 kg_{H2}/day and those for reach stackers, cranes, and yard tractors with a dispensing capacity of 1200 kg_{H2}/day. Peak hourly capacity of both types of HRSs is also taken into account in the model in order not to exceed it [55–57]. In particular, for cars and forklifts the maximum hourly flow rate (i.e. the hourly dispensing capacities) of hydrogen dispensed is about 8 kg_{H2}/h, while for reach stackers, cranes, and yard tractors is about 200 kg_{H2}/h [55–57]. Techno-economic data of HRSs are reported in the Supplementary Material. In the example of Fig. 2, for a group of forklifts, every 2 h one of them is filled with hydrogen (5 kg_{H2}).

Diesel and hybrid Diesel equipment and vehicles are refuelled by Diesel refuelling stations that are already installed in port areas. In the example of Fig. 2, for a group of Diesel forklifts, every 2 h one of them is filled with Diesel (35 kg). Diesel required by the Diesel forklift is higher than that of hybrid Diesel one (about 25 kg).

Definition of energy and market scenarios

The impact of different decarbonization strategies for the energy system of the Industrial Port Area (IPA) is assessed by considering two substructures derived from the superstructure shown in Fig. 3:

1) The first substructure ("*Ind + Equip&Veh*") considers the energy demand of both industry and port vehicles/equipment.

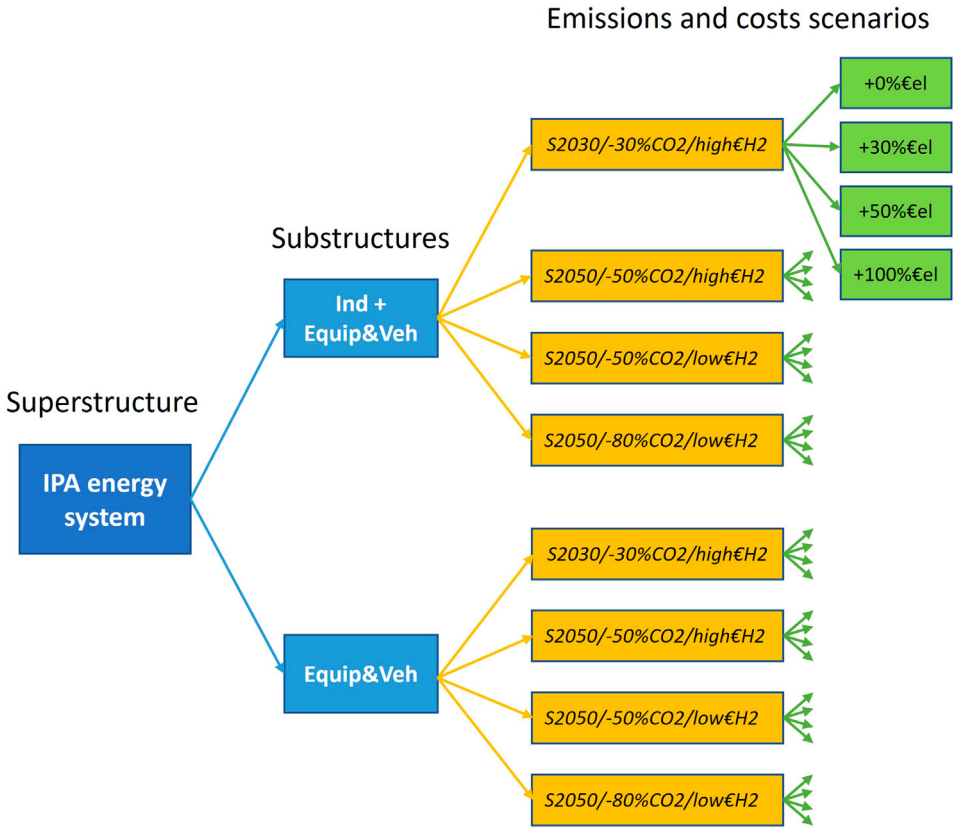

Fig. 3 – Tree diagram for the definition of the energy and market frameworks of the analysis.

2) The second substructure ("*Equip&Veh*") only considers the energy demand of port vehicles/equipment.

For both substructures, different scenarios of emission targets and costs in 2030 and 2050 are considered. In particular:

- in 2030 (*S2030*), emissions are assumed to decrease by 30% from current values (*−30%CO$_2$*), and the costs of all energy conversion and storage units and infrastructures are taken from literature forecasts (see the Supplementary Material), as are the prices of imported H_2, which are shown as "*high€H2*" to highlight their higher values than in 2050.
- in 2050 (*S2050*), emissions are assumed to decrease by 50% (*−50%CO$_2$*) or 80% (*−80%CO$_2$*) from current values, and the costs of all energy conversion and storage units and infrastructures are still taken from literature forecasts (see the Supplementary Material), as are the prices of imported H_2, which are shown here as "*low€H2*" to highlight their lower values than in 2030.

The targets of emission reduction are evaluated from the current value of emissions, which derives from Diesel-fuelled vehicles and equipment, and from grey H_2 imported via trucks and supplied to industry. The target for 2030 (−30%) is in line with scenarios proposed in Ref. [58], while two targets for 2050 (−50% and −80%) are chosen to account for the higher uncertainty associated with a more distant future [1,58].

The scenarios in 2050 include Scenarios *S2050/ … /high€H2* in which the cost of hydrogen remains the same as in 2030, to reflect also the uncertainty on the hydrogen cost in future decades. In both 2030 and 2050, in addition to the options mentioned above, possible increases in the costs of electric vehicles and charging stations (+30%, +50%, and +100%) over those projected were considered in order to assess possible uncertainties in the costs and performance (e.g., range, battery capacity degradation, and battery life) of these vehicles.

The total number of optimization runs according to all the options mentioned above is therefore thirty-two. Fig. 3 shows all these runs and specifies the phrase used to indicate each scenario. For instance, in the S2030/-30%CO2/high€H2 the input scenario (*S*) considers cost data in 2030 (*2030*), a $CO_{2,eq}$ reduction target of 30% compared to the current values (*−30%CO2*) and the cost of imported hydrogen carriers in that year (*highH2*).

Modelling and optimization

Mixed Integer NonLinear Programming (MINLP) is a widely employed method in energy system optimization that best describes the operation of each energy conversion and storage unit within the energy system. However, the use of MINLP approaches can be computationally demanding when dealing with macro energy system comprising multiple interconnected energy units because of the high number of real and integer decision variables associated with their design and operation [59,60]. To address this issue, several authors [61,62] propose to simplify the MINLP into a MILP approach, in which both nonlinear characteristic curves and constraints associated with the energy units can be linearized without substantial loss of accuracy [23,60,63,64]. Accordingly, the computational effort required for the design and operation optimization of the energy system is significantly reduced. Given the complexity of the superstructure under analysis (Fig. 1) and the nature of the optimization problem (dynamic, considering one-year operation), this work makes use of a MILP approach.

The general MILP optimization problem is formulated as in Eq. (1) [65]:

$$\underbrace{\min}_{x,y}\left(\boldsymbol{c}^T\boldsymbol{x}+\boldsymbol{d}^T\boldsymbol{y}\right)\text{s.t.}\quad \boldsymbol{A}\boldsymbol{x}+\boldsymbol{B}\boldsymbol{y}=\boldsymbol{b}\ \text{where}\ \boldsymbol{x}\geq\boldsymbol{0}\in\mathbb{R}^{N_x},\boldsymbol{y}\in\{0,1\}^{N_y} \tag{1}$$

in which c and d are the cost arrays associated with the continuous and binary variables, x and y, respectively; A and B are the equality constraint matrices and b is the constraint known term; N_x and N_y indicate the dimension of x and y, respectively.

The design-operation optimization problem of the energy system shown in Fig. 1 and is formulated considering the following objective function, decision variables and constraints:

- Objective function: the total cost of the system (that is minimized);
- Decision variables: continuous, integer, and binary variables associated with the design and operation of the energy system.
- Constraints: equalities and inequalities associated with the performance and operational limits of the energy conversion and storage units, and the environmental constraint on the total CO_2 emission of the system that must be lower than or equal to reference values imposed by the legislation.

The optimization problem is implemented in Python programming language [66] and solved with the optimizer Gurobi [67].

Following, Section Model of energy conversion and storage units presents the equations and inequalities that describe the design and operation of the energy system components. Section Energy and mass balances of the total system introduces the overall energy and mass balances. Section Powertrain options for port equipment and vehicles focuses on the selection of the best powertrain option for each type and group of equipment and vehicles. Section Objective Function, Decision Variables and $CO_{2,eq}$ Emission Constraint reports objective function, decision variables and the constraint that limits the emission of $CO_{2,eq}$.

Model of energy conversion and storage units

This Section presents the model of the energy system components, introducing the equations that describe the design and operation characteristics of photovoltaic panels (PV), wind turbines (WT), electrolyzer (PEME), compressors (COMP), hydrogen refuelling station (HRS), electric storage system (ESS) and hydrogen storage system (HS). In the following equations, for the j-th energy component, D_j variables define the design variables, δ_j the binary variables identifying the on/

off status or the inclusion/exclusion, P_j the continuous variables identifying electric power flows and H_j the continuous variables identifying the H_2 mass flows.

Crystalline silicon PV panels have chosen to be installed on the roofs of warehouses and buildings in the IPA, as one of the mainly used PV technologies in both stand-alone and on-grid system applications.

The hourly power generated over the year by the PV plant is:

$$P_{PV}(t) = P_{kW_P}(t) \cdot D_{PV} \quad (2)$$

where P_{kW_P} (kwh_e/kW_p) is the specific hourly producibility - i.e., the produced electric energy per kW of peak capacity - and D_{PV} (kW_p) the plant size. P_{kW_P} is evaluated by *PVGIS Tool* [68], considering an average hourly solar irradiance and an optimum oriented PV module in Trieste, considering system losses of about 14%. The constraint on the PV plant size due to the limited available area is:

$$D_{PV} \leq A_{PV,max} / coef_{PV} \quad (3)$$

where $A_{PV,max}$ (m^2) is the maximum available area in the port (160.000 m^2) and $coef_{PV}$ (m^2/kW_p) is the peak power specific area.

Wind turbines

Six models of horizontal-axis WT are identified for installation in possible sites of the port area, with rated powers ranging from 10 kW to 1 MW. In the Supplementary Material, Table A.4 reports the main characteristics of the six types of WT chosen from different commercial applications. A maximum number of ten WT of the same type is set.

The power $P_{w_i}(t)$ (kW) generated by a single turbine is calculated from its power-wind velocity characteristic curve. In case the wind velocity is not within the $v_{cut,in}$ - $v_{cut,off}$ interval, there is no power generation. The hourly wind velocity is estimated by PVGIS tool [68].

The total power generated by the wind farm is:

$$P_w(t) = \sum_i \delta_{w_i} \cdot P_{w_i}(t) \quad (4)$$

being δ_{w_i} the binary variable identifying the inclusion/exclusion of the i-th WT in the energy system.

Proton Exchange Membrane Electrolyzer

A PEME technology is here selected as technology to be installed in the IPA to produce H_2 via water electrolysis. Differently from alkaline electrolyzers, PEMEs well bear intermittent operation, guarantee high purity in the outward H_2 and reach higher efficiency levels. In Eq. (5), the mass flow rate ($\dot{H}_{LP,elect}$, kg/h) of H_2 produced at 30 bar by the electrolyzer is defined as function of the power absorbed by the PEME (P_{elect}, kW), and a proportionality coefficient (k_{elect}), which is determined according to the linearization of the performance curve of a typical PEME at different power load. δ_{elect} is the binary variable accounting for the on/off status of the electrolyzer. The absorbed electric power is constrained in Eq. (6) not to exceed the power load range. The power bounds are expressed as percentages $k_{\min\ elect}$ and $k_{\max\ elect}$ of the electrolyzer nominal power D_{elect} (kW).

$$\dot{H}_{LP,elect}(t) = k_{elect} \cdot P_{elect}(t) \cdot \delta_{elect}(t) \quad (5)$$

$$k_{min\ elect} \cdot D_{elect} \leq P_{elect}(t) \leq k_{\max\ elect} \cdot D_{elect} \quad (6)$$

Low pressure and high pressure compressors

The compression station makes use of single stage reciprocating compressors operating between 30 and 300 bar for the lower pressure level and between 300 and 820 bar for the higher one. The advantage of reciprocating compressors compared to centrifugal ones is three-fold: (i) allow higher pressure ratios, (ii) are more robust and have longer lifetimes and (iii) sealings are better suited to the properties of H_2 (small molecule, high diffusivity).

The electric power P_{comp} (kW) absorbed by a compressor is calculated starting from the specific work of the adiabatic isentropic compression $L_{comp,is}$ (kJ/kg)

$$P_{comp}(t) = \dot{H}(t) \cdot \frac{L_{comp,id}}{\eta_{is} \cdot \eta_{mech} \cdot \eta_{el}} \cdot \delta_{comp}(t) \quad (7)$$

being η_{is} and η_{mech} the isentropic efficiency and the mechanical efficiency of the compressor, and η_{el} the efficiency of the electric motor driving the compressor. δ_{comp} is the binary variable that defines the on/off status of the compressors.

The calculation of the specific work of the adiabatic isentropic compression assumes H_2 is approximated to a monoatomic ideal gas and the constant pressure specific heat capacity c_P does not depend on the temperature and is directly related to the specific gas constant as expressed in Eq. (8).

$$c_P = \frac{\gamma}{\gamma - 1} \cdot R \quad (8)$$

Similarly to the electrolyzer, the power of the compressor is constrained not to exceed the power load range. Where the power bounds are expressed as percentages $k_{\min\ comp}$ and $k_{\max\ comp}$ of the compressor nominal power D_{comp} (kW).

$$k_{\min\ comp} \cdot D_{comp} \leq P_{comp}(t) \leq k_{\max\ comp} \cdot D_{comp} \quad (9)$$

Hydrogen Refuelling Stations

HRS are divided into two types: one dedicated to the refuelling of light-duty vehicles and one to heavy-duty equipment and vehicles. The two different types differ only by the maximum capacity to supply H_2 to equipment and vehicles in terms of kg supplied per hour and per day, and costs. HRS are included in the energy system when a specific group of hybrid hydrogen equipment and vehicles is chosen as optimal solution. HP hydrogen storage supplies H_2 to the HRS at 820 bar. This pressure is high enough such that HRS does not need an additional compressor unit to supply H_2 equipment and vehicles assuming they have an on-board H_2 tank operating at 700 bar pressure. Each HRS is equipped with a refrigerator unit, which cools down the H_2 to −40 °C, avoids the heating of the H_2 and, in turn, ensures full fillings of the on-board equipment and vehicle tanks and avoid safety issues (referring to the standard SAE-J2601 [32]). The only energy demand of HRS operation is the electric power P_{refr} (kW) for the refrigeration of H_2 mass flow rate required by the j-th group of equipment and vehicles ($\dot{H}_{j,vehicle}$, kg/h).

$$P_{refr}(t) = \frac{\dot{H}_{j,vehicle}(t) \cdot (h_{storage} - h_{dispenser})}{COP} \quad (10)$$

where COP is the coefficient of performance and $h_{storage}$ and $h_{dispenser}$ are the H_2 enthalpies in the HP storage and at the dispenser outlet, respectively.

Electric storage system

Stationary Li-ion batteries are used to store electric energy. They are chosen between other electric storage solutions (e.g. lead-acid batteries and capacitors) as good compromise between costs, energy density, voltage fluctuations of the output power and modularity [69].

The integral form of the electric energy balance at the electric storage is

$$E_{batt}(t) = E_{batt}(t-\Delta t) + \eta_{batt} \cdot P^{-}_{batt}(t-\Delta t)\Delta t - (1/\eta_{batt}) \cdot P^{+}_{batt}(t-\Delta t)\Delta t \quad (11)$$

which states that the electric energy in the storage $E_{batt}(t)$ (kWh) at time t is equal to the electric energy in the storage $E_{batt}(t-\Delta t)$ (kWh) at the preceding time plus/minus the electric power entering to (P^{-}_{batt}, kW) or exiting from (P^{+}_{batt}, kW) the storage multiplied by the time step (Δt, h). η_{batt} is the charging/discharging efficiency.

The electric energy in the storage lies between a minimum and a maximum state of charge, which are set as percentages ($k_{\min\ batt}$ and $k_{\max\ batt}$) of the battery design capacity (D_{batt}, kWh).

$$k_{\min\ batt} \cdot D_{batt} \le E_{batt}(t) \le k_{\max\ batt} \cdot D_{batt} \quad (12)$$

Moreover, the stored electric energy at the first-time step must equal that at the end of the simulation period.

$$E_{batt}(0) = E_{batt}(t_{end}) \quad (13)$$

Low pressure and high pressure hydrogen storage

The integral form of the mass balance at the LP hydrogen storage (Eq. (14)) and at the High-Pressure (HP) hydrogen storage (Eq. (15)) are:

$$H_{S_{LP}}(t) = H_{S_{LP}}(t-\Delta t) + \dot{H}_{inLP}(t-\Delta t)\Delta t - \dot{H}_{outLP}(t-\Delta t)\Delta t - \dot{H}_{out,ind}(t-\Delta t)\Delta t \quad (14)$$

$$H_{S_{HP}}(t) = H_{S_{HP}}(t-\Delta t) + \dot{H}_{inHP}(t-\Delta t)\Delta t - \dot{H}_{out,vehicle}(t-\Delta t)\Delta t \quad (15)$$

which states that the mass in the storage $H_{S_{LP}}(t)$ and $H_{S_{HP}}(t)$ (kg) at time t is equal to the mass in the storage $H_{S_{LP}}(t-\Delta t)$ and $H_{S_{HP}}(t-\Delta t)$ (kg) at the preceding time plus/minus the mass flow rates entering to ($\dot{H}_{inLP}$ and $\dot{H}_{inHP}$, kg/h) or exiting from ($\dot{H}_{outLP}$, $\dot{H}_{out,ind}$, $\dot{H}_{out,vehicle}$, kg/h) the storage multiplied by the time step (Δt, h).

For both the LP and HP hydrogen storage, the mass in the storage varies between a minimum and a maximum set as percentages (k_{minHS} and k_{maxHS}, %) of the storage design capacity ($D_{S_{LP}}$ and $D_{S_{HP}}$, kg) (Eqs. 16 and 17). Moreover, the stored mass at the first-time step must equal that at the end of the simulation period, i.e. a year operation (Eqs. 18 and 19).

$$k_{minHS} \cdot D_{S_{LP}} \le H_{S_{LP}}(t) \le k_{maxHS} \cdot D_{S_{LP}} \quad (16)$$

$$k_{minHS} \cdot D_{S_{HP}} \le H_{S_{HP}}(t) \le k_{max\ HS} \cdot D_{S_{HP}} \quad (17)$$

$$H_{S\ LP}(0) = H_{S\ LP}(t_{fin}) \quad (18)$$

$$H_{S\ HP}(0) = H_{S\ HP}(t_{fin}) \quad (19)$$

Energy and mass balances of the total system

The energy management system sets out the power flows between the energy units. The electric power balance states the equivalence of the power generation and consumption. It reads

$$\sum_{t=0}^{t_{fin}} \left(P_{PV}(t) + P_w(t) + P^{+}_{GRID}(t) - P^{-}_{GRID}(t)\right) = \sum_{t=0}^{t_{fin}} \left(P_{elect}(t) + P_{comp_{LP}}(t) + P_{comp_{HP}}(t) + P_{refr}(t) + \sum_{v}\sum_{gp} P^{v}_{gp,2}(t)\delta^{v}_{gp,2} \right) \quad (20)$$

where $P_{PV}(t)$ and $P_w(t)$ are the power generated by the PV plant and the WT, respectively. $P^{+}_{GRID}(t)$ and $P^{-}_{GRID}(t)$ are the electric power purchased from and sold to the national grid, respectively. $P_{elect}(t)$ is the input power of the electrolyzer, $P_{comp_{LP}}(t)$ is the input power of the LP compressor and $P_{compHP}(t)$ is the input power of the HP compressor. $P_{refrig}(t)$ is the power required by the refrigeration units, and $P_{vehicles}(t)$ is the power to recharge full electric equipment and vehicles. *v* is the index of *equipment and vehicle type*, *gp* is the index of equipment and vehicles group.

The mass balance for H2 flows is:

$$\sum_{t=0}^{t_{fin}} \left(\left(H_{LP,elect}(t) + H_{GH_2,trucks}(t) + H_{LH_2,ships}(t) + H_{NH_3,ships}\ (t)\right) \right) = \sum_{t=0}^{t_{fin}} H_{ind}(t) + \sum_{t=0}^{t_{fin}} \sum_{v}\sum_{gp} H^{v}_{gp,1}(t) \cdot \delta^{v}_{gp,1} \quad (21)$$

$H_{LP,elect}(t)$ is the H_2 produced by the electrolyzer at time t, $H_{GH_2,trucks}(t)$, $H_{LH_2,ships}(t)$ and $H_{NH_3,ships}$ (t) are the flows of H_2 imported as GH_2 via trucks, as LH_2 via ships, and as NH_3 via ships, respectively. The mass flow of H_2 locally produced and/or imported equals that requested by the industry and by the equipment and vehicles (if hybrid H_2 powertrain is chosen as optimal option for the gp-th groups of the v-th types of equipment and vehicles). Note that in the overall energy and mass balances (Eqs. (20)–(22)) the terms accounting for the variation of storage levels (i.e., battery storage and hydrogen tanks) do not appear because of constraints in Eqs. (13), (18) and (19).

Similarly, the mass balance for Diesel flows is:

$$\sum_{t=0}^{t_{fin}} F_{vehicles}(t) = \sum_{t=0}^{t_{fin}} \sum_{v}\sum_{gp} H^{v}_{gp,3}(t) \cdot \delta^{v}_{gp,3} + \sum_{t=0}^{t_{fin}} \sum_{v}\sum_{gp} H^{v}_{gp,4}(t) \cdot \delta^{v}_{gp,4} \quad (22)$$

The amount of Diesel entering in the energy system ($F_{vehicles}$) equals that requested by conventional Diesel (pt = 3) and/or hybrid Diesel (pt = 4) equipment and vehicles (if Diesel-

powered powertrain are chosen as optimal options for the gp-th groups of the v-th types of equipment and vehicles).

Powertrain options for port equipment and vehicles

The choice of the optimal *powertrain* for an equipment and vehicle *group* is one of the main goals of this study strongly affecting the H_2/energy demands of port equipment and vehicles. To limit the increase of the number of binary variables and to comply with the performance characteristics of HRS, equipment and vehicles of the same type are grouped as described in Section Energy and hydrogen demands, and binary variables are used to choose a specific *powertrain (pt)* for each *group (gp)* of each *equipment and vehicle type (v)*. For each type of equipment and vehicle v (i.e., cars, cranes, reach stackers, forklifts, and yard tractors), a matrix of binary variables y^v is defined as reported in Eq. (23):

$$y^v = \begin{bmatrix} \delta^v_{1,1} & \cdots & \delta^v_{1,pt} \\ \vdots & \vdots & \vdots \\ \delta^v_{gp,1} & \cdots & \delta^v_{gp,pt} \end{bmatrix} \tag{23}$$

where rows represent the groups (*gp*) and columns the corresponding powertrains (*pt*). The four powertrains are listed as: hybrid H_2 ($pt = 1$), full-electric ($pt = 2$), Diesel ($pt = 3$), or hybrid Diesel ($pt = 4$). For instance, the dimension of the above matrix for tractors is 3 (*groups*) x 4 (*powertrains*). Given the definition of *group* introduced in Section Energy and hydrogen demands, the sum of the elements of each row in each matrix y^v is equal to one because a *group* of equipment and vehicles is identified by one optimal *powertrain* only.

Objective function, decision variables and $CO_{2,eq}$ emission Constraint

This Section presents the objective function of the optimization model and the constraint that limits the $CO_{2,eq}$ emissions of the energy system.

The optimizer seeks for a minimum of the sum of annualized investment, replacement, operation and management cost, plus the operation cost related to the energy flow entering and outgoing from the energy system. Thus, the objective function (f_{Obj}, €/y) reads

$$f_{Obj} = \sum_j D_j \left(C_{inv,a_j} + C_{rep,a_j} + C_{O\&M_j} \right) + \sum_j c_j \left(P_{in_j} + H_{in_j} + F_{in_j} - P_{out_j} \right) \tag{24}$$

For each j-th energy component (i.e., PV, WT, PEME, ESS, compressor, hydrogen storage system, H_2 refuelling station, refrigeration unit and vehicles), the decision variables are: design variables "D_j" (kW, kg or kWh), power flows "P_j" (kWh), Diesel mass flows "F_j" (kg), hydrogen mass flows "H_j" (kg), and binary variables "δ_j". The latter control the on/off status or the inclusion/exclusion of the j-th unit.

C_{inv,a_j} (€ per kW per year or € per kg per year or € per kWh per year) and C_{rep,a_j} (€ per kW per year or € per kg per year or € per kWh per year) are the annualized investment and replacement specific costs, respectively. $C_{O\&M_j}$ (€ per kW per year or € per kg per year or € per kWh per year) are the operation and maintenance specific costs.

c_j (€ per kWh or kg of fuel) are the cost and related to the corresponding input and output mass and energy flows that enter/exit from the j-th component (P_{in_j} (kWh), H_{in_j} (kg), F_{in_j} (kg), P_{out_j} (kWh)), defined respectively in kWh of electricity, kg of hydrogen, kg of diesel and kWh of electricity).

Annualized investment, replacement and operation and maintenance costs are evaluated as proposed in Ref. [70], considering a 25-year operating life of the energy system and a 5% discount rate.

The constraint on the $CO_{2,eq}$ emissions imposes an upper bound on the emission from the industrial port area

$$\sum_j \left(e_{CO2,eq_j} \cdot \left(P_{in_j} + H_{in_j} + F_{in_j} \right) \right) \leq (1 - E_{\%}) \cdot E_{TOT,ref} \tag{25}$$

where e_{CO2,eq_j} ($kg_{CO2,eq}$ per kWh or kg of fuel) is the carbon footprint related to each energy and mass flow entering the energy system model, $E_{TOT,ref}$ ($kg_{CO2,eq}$ per year) is the total $CO_{2,eq}$ emission of the baseline scenario and $E_{\%}$ is the percentage reduction. Eq. (25) allows to set the decarbonization goals with respect to the current configuration (baseline) in which all equipment and vehicles are powered by Diesel internal combustion engines, the steel industry H_2 demand is met by grey H_2 imported via trucks and PV, WT, electric storage systems and electrolysers are not present.

Note that the "green" electricity generated by PV and WT is either used internally or sold to the grid. The resulting "grid decarbonization" effect is not accounted here for the sake of simplicity, thus the obtained decarbonization levels are actually underestimated.

Optimization results and discussion

This Section presents the main results of the industrial port area optimization. In particular, Section Substructure including industry, port equipment and vehicles energy demand reports the optimization of the energy system of the IPA substructure which includes the energy demands of both industry and port equipment and vehicles. Section Substructure including only port equipment and vehicles energy demand presents the results related to the optimization of the energy system of the IPA substructure without the industry (i.e., including only the energy demands of the port equipment and vehicles). Section Comparison of the two substructures and critical remarks provides a comparative analysis of the results of the two substructures and discusses the main findings. In the following, the various results of the optimization simulations are also compared to a current reference Scenario "0", in which port equipment and vehicles are Diesel-fuelled and the H_2 for the industry is grey H_2 imported via trucks.

Substructure including industry, port equipment and vehicles energy demand

This Section considers the substructure including the energy demands of both the industry and port equipment and vehicles. Fig. 4 shows the percentages of the different contributions to carbon emissions in the reference Scenario 0. The grey H_2 for the steel industry is imported via trucks and accounts

for approximately 27% of the total emissions in the IPA, corresponding to about 10,000 $tCO_{2,eq}$/year. Among equipment and vehicles, tractors are responsible for 51% of the total emissions, while stackers and cranes account for approximately 11% and 9%, respectively. Forklifts and cars have the lowest Diesel consumption over the year and contribute to just 2% and 0.1% of the total emissions, respectively.

For a given future scenario (Section Definition of energy and market scenarios), the optimizer provides the optimal configuration of the equipment and vehicles fleet, i.e., the optimal powertrain for each group and type of equipment and vehicles. Fig. 5 shows the energy required (left axis) by port equipment and vehicles in the different scenarios and cases (horizontal axis). Grey solid and chessboard bars represent the energy demand of Diesel and hybrid Diesel powertrains, respectively. Red dotted bars refer to the energy required by battery electric equipment and vehicles, while blue wave bars to the energy demand of hydrogen equipment and vehicles.

Given the high impact of Diesel equipment and vehicles on the total $CO_{2,eq}$ emissions of the IPA, Diesel powertrains are the first to be replaced with less environmentally impactful powertrain options when an emission reduction is required. This replacement is apparent in Fig. 5 moving from the baseline case (Scenario 0) to the *S2030/-30%CO2/high€H2* scenario where most of the Diesel equipment and vehicles are substituted by hybrid Diesel ones. Despite a slight increase of costs, the use of batteries in the hybrid Diesel option allows a sufficient emission reduction to meet the 30% target of emission reduction in the 2030 scenario.

In 2050, the cost reduction of hydrogen equipment and vehicles, as well as the stricter constraint on $CO_{2,eq}$ emissions, bring hydrogen equipment and vehicles into the optimal configuration of equipment and vehicles. The two scenarios with a 50% $CO_{2,eq}$ emission reduction target (S2050/-50%CO2/high€H2 and *S2050/-50%CO2/low€H2*) differ in the origin and price of H_2. In *S2050/-50%CO2/high€H2*, optimizer chooses to import most of the H_2 needed as grey H_2 imported by truck, mainly because its cost is lower than that of green H_2. In *S2050/-50%CO2/low€H2*, on the other hand, the overall cost of green H_2 is lower than that in the *S2050/-50%CO2/high€H2*, but the percentage of H_2 demand for equipment and vehicles is reduced because a 50% $CO_{2,eq}$ emission reduction is achieved by importing NH_3 to meet the industry H_2 demand. NH_3, as imported H_2 carrier, is selected instead of LH_2 for the IPA, due to its predicted lower future cost and carbon footprint. In both 2050 scenarios with 50% reduction of emissions (i.e., *S2050/-50%CO2/high€H2* and *S2050/-50%CO2/low€H2*), Hybrid Diesel equipment and vehicles constitute a large share of the energy demand of equipment and vehicles, although electric equipment and vehicles are more convenient in terms of emission reduction when their cost is not too high and they can exploit PV energy. As the cost of electric equipment and vehicles increases, their share in the optimal equipment and vehicle fleet reduces and the relative share of hydrogen equipment and vehicles increases. In *S2050/-50%CO2/high€H2* scenario, the energy demand of electric equipment and vehicles decreases gradually from the case *0%€el* to the *+100%€el* one, whereas in *S2050/-50%CO2/low€H2* scenario the electric equipment and vehicles disappear from *+30%€el* upwards. The increase of the energy demand of equipment and vehicles from *S2050/-50%CO2/high€H2* to *S2050/-50%CO2/low€H2* is mainly due to the rise of the share of hybrid Diesel equipment and vehicles. In *S2050/-80%CO2/low€H2*, if the cost of battery electric equipment and vehicles exceeds the predicted cost by at least 30%, the most cost-effective way to achieve the 80% reduction of emissions is the conversion of almost all equipment and vehicles into hydrogen ones. Being the relative weight of cars not significant in the total account of emissions, the conversion of Diesel cars into other powertrain options is not cost-effective in any of the defined scenarios and cases.

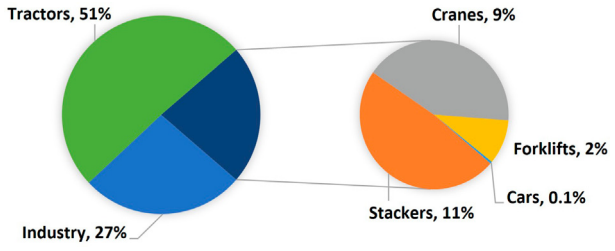

Fig. 4 – Current contributions to carbon emissions related to the operation of industry and port equipment and vehicles in the reference Scenario 0.

In all scenarios, the total energy demand of the equipment and vehicle fleet is lower than that of the Scenario 0 because the alternative powertrain options are more efficient than conventional Diesel one. Focusing on *S2050/-50%CO2/high€H2* in Fig. 5, further considerations can be made about the efficiencies of the different powertrains. In case the cost of electric equipment and vehicles equals the predicted one (*0%€el*), the electric equipment and vehicles concur to about one-third of the energy demand and the total energy demand is the lowest within this scenario. The low energy demand (see also case *0%€el* in *S2050/-80%CO2/low€H2* scenario) is a consequence of the energy conversion efficiency of the electric equipment and vehicle, which is the highest among all the powertrains. This is also confirmed by the decrease of the number of electric equipment and vehicles, as the cost of the electric equipment and vehicle increases.

This observation is confirmed also by the fact that, as the cost of the electric equipment and vehicles increases, the number of electric equipment and vehicles decreases and, in turn, the energy demand increases. The use of hydrogen equipment and vehicles decreases the energy demand as highlighted by the *S2050/-50%CO2/high€H2* and *S2030/-30% CO2/high€H2* comparison. So, hydrogen equipment and vehicles have a value of energy conversion efficiency that is in between that of hybrid Diesel equipment and vehicles and that of electric ones.

Fig. 6 shows the composition of H_2 supplied to the steel industry and to equipment and vehicles (in case that some groups of equipment and vehicles powered by H_2 appear in the optimal fleet) for the different scenarios and cases. Grey solid bars represent grey H_2, whereas green chessboard bars and orange diagonal-stripe bars represent locally produced and imported H_2, respectively. The blue dotted line highlights the constant H_2 amount of 1000 tons of H_2 per year required by the industry. A bar exceeding this line indicates that some

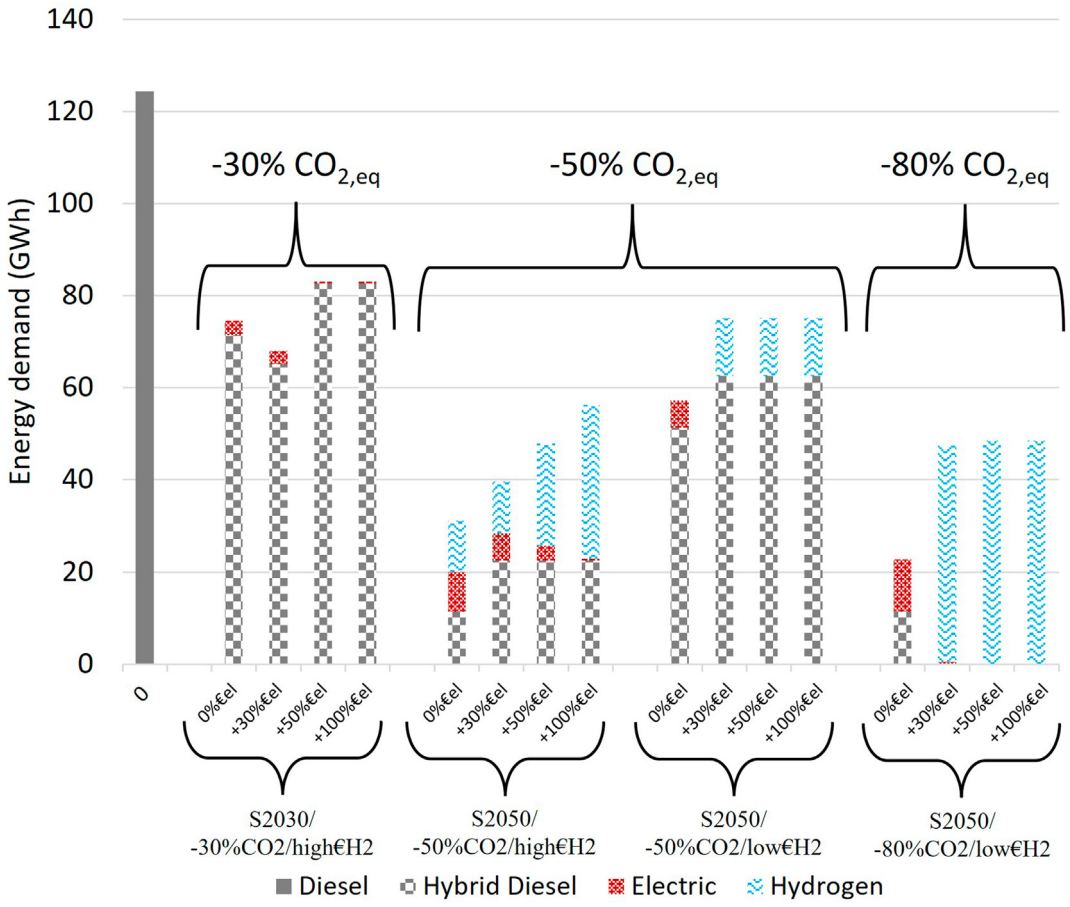

Fig. 5 – Composition of the energy required by port equipment and vehicles (bars, left axis) and $CO_{2,eq}$ emissions (line, right axis), in the different scenarios and cases, for the substructure with both industry and port equipment and vehicles. Grey solid and grey chessboard bars represent the energy demand of Diesel and hybrid Diesel powertrains, respectively. Red dotted bars refer to the energy required by battery electric equipment and vehicles, while blue wave bars to the energy demand of hydrogen equipment and vehicles. (For interpretation of the references to colour in this figure legend, the reader is referred to the Web version of this article.)

hydrogen equipment and vehicles have been included in the optimal fleet.

When the cost of imported NH_3 refers to 2030 (scenarios with "*high€H2*" label), local production of H_2 is a viable decarbonization option only if the cost of equipment and battery electric vehicles is higher than that predicted for 2030 and 2050, i.e., at least 50% higher in *S2030/-30%CO2/high€H2* and at least 30% higher in *S2050/-50%CO2/high€H2*. According to the costs of technologies to produce, compress and store H_2, of power purchased from the grid, and of renewable power production, no more than 323 tons of H_2 per year are produced locally. In this case, a 5.9 MW sized electrolyzer is selected; its percentage utilisation factor reaches 33%.

In the scenario S2030/-30%CO2/high€H2, locally produced hydrogen has an average annual carbon footprint below 0.4 $kg_{CO2,eq}/kg_{H2}$ and production costs of 8.8 €/kg_{H2} and 9.9 €/kg_{H2} when considering a +50% and +100% higher cost of electric battery vehicles, respectively. Local hydrogen production is preferred to the import of ammonia because of the much lower carbon footprint (0.4 $kg_{CO2,eq}/kg_{H2}$ versus 2.5 $kg_{CO2,eq}/kg_{H2}$), in spite of the higher cost (8.8 €/kg_{H2} or 9.9 €/kg_{H2} versus 4.55 €/kg_{H2} of ammonia).

In the case of S2050/-50%CO2/high€H2, the costs (and carbon footprint) for locally produced hydrogen are about 7.6 €/kg_{H2} (2.39 $kg_{CO2,eq}/kg_{H2}$), 4.0 €/kg_{H2} (1.17 $kg_{CO2,eq}/kg_{H2}$), and 3.9 €/kg_{H2} (0.75 $kg_{CO2,eq}/kg_{H2}$) when assuming a +30%, +50%, and +100% higher cost of electric battery vehicles, respectively.

In "*low€H2*" scenarios, NH_3 gives the most substantial contribution in decarbonizing both industry and port equipment and vehicles. If 80% reduction of emissions is required (*S2050/-80%CO2/low€H2*), imported NH_3 covers the entire industrial demand of H_2 but it becomes the only refuelling option for all equipment and vehicles, except the cars, if electric equipment and vehicles have at least a cost 30% higher respect to the predicted one.

Despite the higher cost of NH_3 (+13% of the grey H_2), it is selected in the low-cost H_2 scenarios (*low€H2*) because of its lower carbon impact (approximately four times lower than grey H_2).

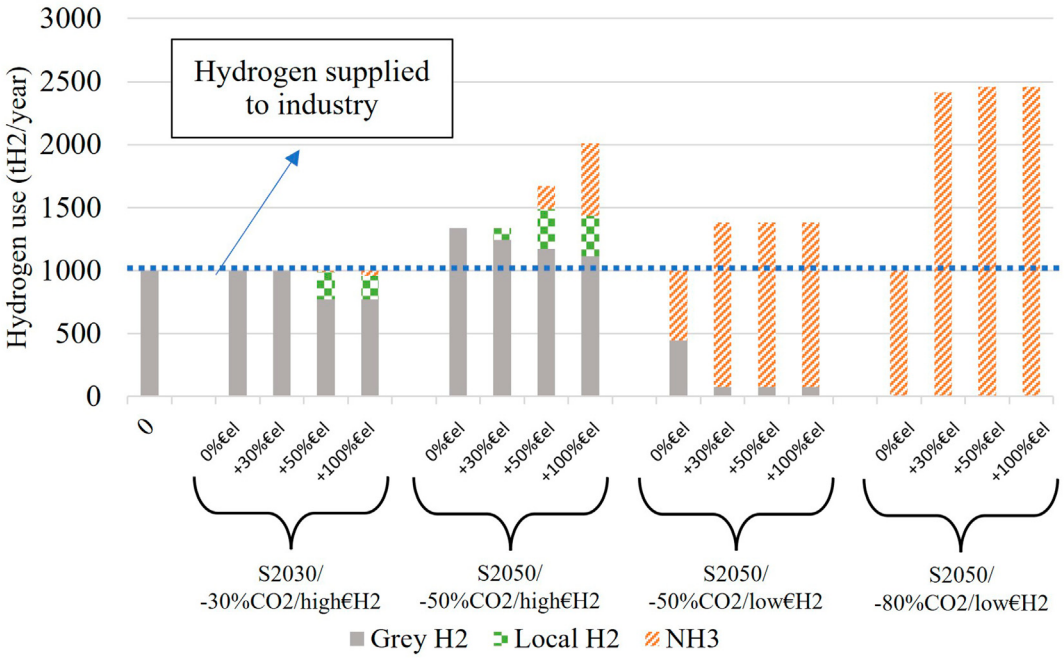

Fig. 6 – Composition of H_2 supplied to the steel industry and to equipment and vehicles, in the different scenarios and cases, for the substructure with both industry and port equipment and vehicles. Grey solid bars represent grey H_2, whereas green chessboard bars and orange diagonal-stripe bars represent locally produced and imported H_2, respectively. The blue dotted line highlights the constant H_2 quantity of 1000 tons of H_2 required per year by the industry. (For interpretation of the references to colour in this figure legend, the reader is referred to the Web version of this article.)

Substructure including only port equipment and vehicles energy demand

The optimization results of the substructure of the IPA with only port equipment and vehicles (without the industry) allows to distinguish the influence of equipment/vehicles and industry in determining the optimal powertrain options for various types of equipment and vehicles.

Fig. 7 shows the same information of Fig. 5 (Section Substructure including industry, port equipment and vehicles energy demand) for the substructure without industry. The left axis shows the values of the energy demands of equipment and vehicles for different scenarios and costs of electric equipment and vehicles, whereas the right axis shows the percentages of emission reduction. The different types of bars keep the same meaning. Similarly to Fig. 6 (Section Substructure including industry, port equipment and vehicles energy demand), Fig. 8 shows the origin of the H_2, i.e., grey, locally produced or imported H_2. The amount of H_2 is only related to hydrogen equipment and vehicles (substructure without industry).

In scenarios where the cost of imported NH_3 is that of 2030 (i.e., *S2030/-30%CO2/high€H2* and *S2050/-50%CO2/high€H2*) hydrogen equipment and vehicles appear when the cost of electric equipment and vehicles is 30% higher than the predicted one and most of the H_2 is grey. In *S2030/-30%CO2/high€H2* scenario, H_2 comes from local production only when the cost of the battery electric equipment and vehicles is twice the predicted cost (*+100%€el*). In this scenario, the average annual carbon footprint of locally produced hydrogen is almost zero (lower than 0.01 $kg_{CO2,eq}/kg_{H2}$), while the cost is about 8.3 €/kg_{H2}. On the other hand, in *S2050/-50%CO2/high€H2* about one-fifth of the H_2 is always produced locally if the cost of battery electric equipment and vehicles is at least 30% higher than the predicted one. The highest local production of H_2 occurs in the scenario *S2050/-50%CO2/high€H2*, in which a 4 MW electrolyser operating at a utilisation factor of about 42% is chosen. In *S2050/-50%CO2/high€H2*, costs (and carbon footprint) are about 6.5 €/kg_{H2} (1.03 $kg_{CO2,eq}/kg_{H2}$), 5.9 €/kg_{H2} (0.99 $kg_{CO2,eq}/kg_{H2}$) and 5.11 €/kg_{H2} (1.22 $kg_{CO2,eq}/kg_{H2}$) when a +30%, +50% and +100% higher cost of electric battery vehicles is assumed, respectively. Despite the slightly higher cost, local production of hydrogen is preferred to imported ammonia because of the lower footprint (values around 1 $kg_{CO2,eq}/kg_{H2}$, as seen above, versus the ammonia carbon footprint of 2.5 $kg_{CO2,eq}/kg_{H2}$).

It is important to note that in scenarios with high costs for H_2 carriers and battery electric equipment and vehicles, grey H_2 imported via trucks may also play a role in decarbonizing port equipment and vehicles. This is because the lower emissions from the hydrogen equipment and vehicles fuelled by grey H_2, compared to those from Diesel and hybrid Diesel powertrains.

Fig. 8 highlights that in scenarios with "*low€H2*" H_2 supply and associated equipment are so convenient that no more electric equipment and vehicles are included in the optimal fleet (even in the cases *0%€el*). In both *S2050/-50%CO2/low€H2* and *S2050/-80%CO2/low€H2* scenarios, most of the H_2 is

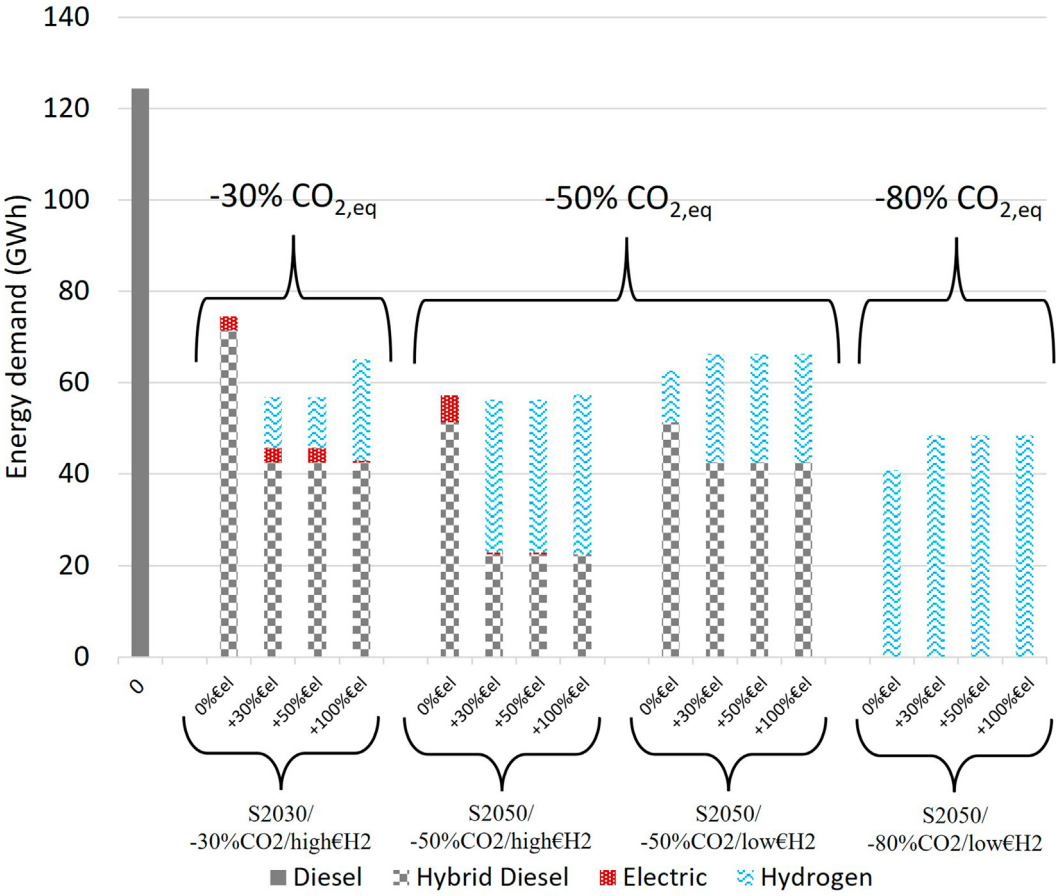

Fig. 7 – Composition of the energy required by port equipment and vehicles (bars, left axis) and $CO_{2,eq}$ emissions (line, right axis), in the different scenarios and cases, for the substructure with only port equipment and vehicles. Grey solid and grey chessboard bars represent the energy demand of Diesel and hybrid Diesel powertrains, respectively. Red dotted bars refer to the energy required by battery electric equipment and vehicles, while blue wave bars to the energy demand of hydrogen equipment and vehicles. (For interpretation of the references to colour in this figure legend, the reader is referred to the Web version of this article.)

imported via NH_3 (Fig. 8). When an 80% reduction of emissions is imposed, H_2 technologies are the preferred option for almost all equipment and vehicles (except for cars) due to the low carbon impact of H_2 imported in the form of NH_3 via ships. Overall, when NH_3 is available at a lower price, hydrogen equipment and vehicles are chosen instead of battery electric equipment and vehicles.

Comparison of the two substructures and critical remarks

In all energy system substructures, scenarios and cases, the capacity of the PV power plant is 20 MW_P, which corresponds to the upper bound constraint. Conversely, the wind turbines are never installed due to the unfavourable wind conditions (highly variable wind speed).

The coefficient of decarbonization ($coef_{decarb}$) is a metric to evaluate the potential decarbonization impact of the proposed decarbonization strategies for the IPA

$$coef_{decarb,i} = \frac{Cost_{tot_i} - Cost_{op_{ref}}}{Em_{op_{ref}} - Em_{tot_i}} \quad (27)$$

The numerator is the difference between the total cost of the optimized system in each scenario i ($Cos\ t_{tot_i}$) and the cost of the reference scenario ($Cos\ t_{op_{ref}}$), and the denominator the difference between the emissions of the reference scenario ($Em_{op_{ref}}$) and those of the optimized system in each scenario i (Em_{tot_i}).

The coefficient is defined in €/$tCO_{2,eq}$ and represents the cost to avoid the emission of a ton of $CO_{2,eq}$ per year in a scenario i. Figs. 9 and 10 show the total costs of the system (bars, left axis) and the related values of the decarbonization coefficient (lines, right axis) of the two energy system substructures with and without industry (solid bars and lines for the substructure with the industry "*Ind + Equip&Veh*", wave bars and dashed lines for the substructure without industry "*Equip&Veh*").

The inclusion of the industry makes the system total costs always higher than those of the substructure including only the port equipment and vehicles (i.e., the solid bars are higher than the wave bars in all cases). Nevertheless, the decarbonization coefficient shows the opposite trend, i.e., it is always higher for the substructure without the industry. Given the

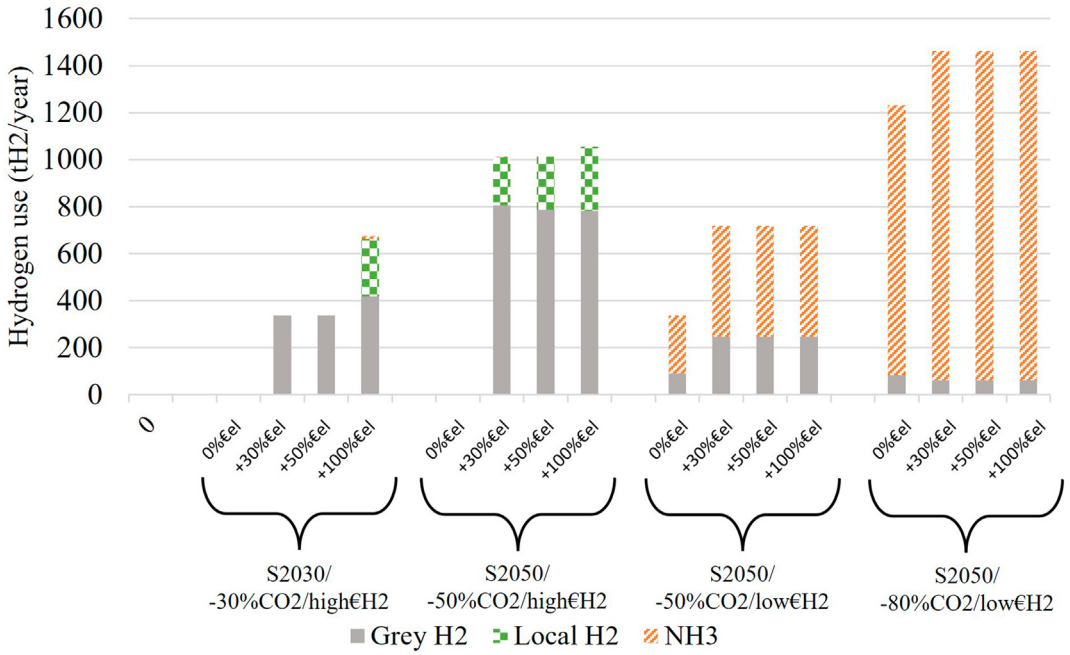

Fig. 8 – Composition of H_2 supplied to only equipment and vehicles in the different scenarios and cases. Grey solid bars represent grey H_2, whereas green chessboard bars and orange diagonal-stripe bars represent locally produced and imported H_2, respectively. (For interpretation of the references to colour in this figure legend, the reader is referred to the Web version of this article.)

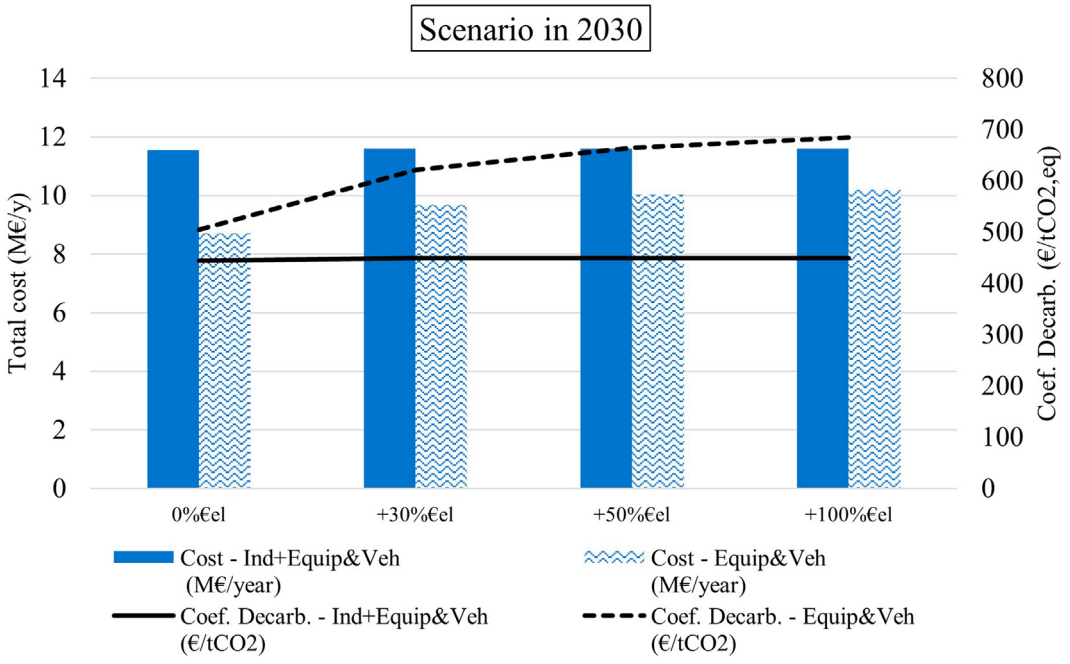

Fig. 9 – Total costs of the system (bars, left axis) and the related decarbonization coefficient (lines, right axis) of the two energy system substructures with and without industry in 2030. Solid bars and lines refer to the substructure with the industry ("Ind + Equip&Veh"), while wave bars and dashed lines to the substructure without industry ("Equip&Veh").

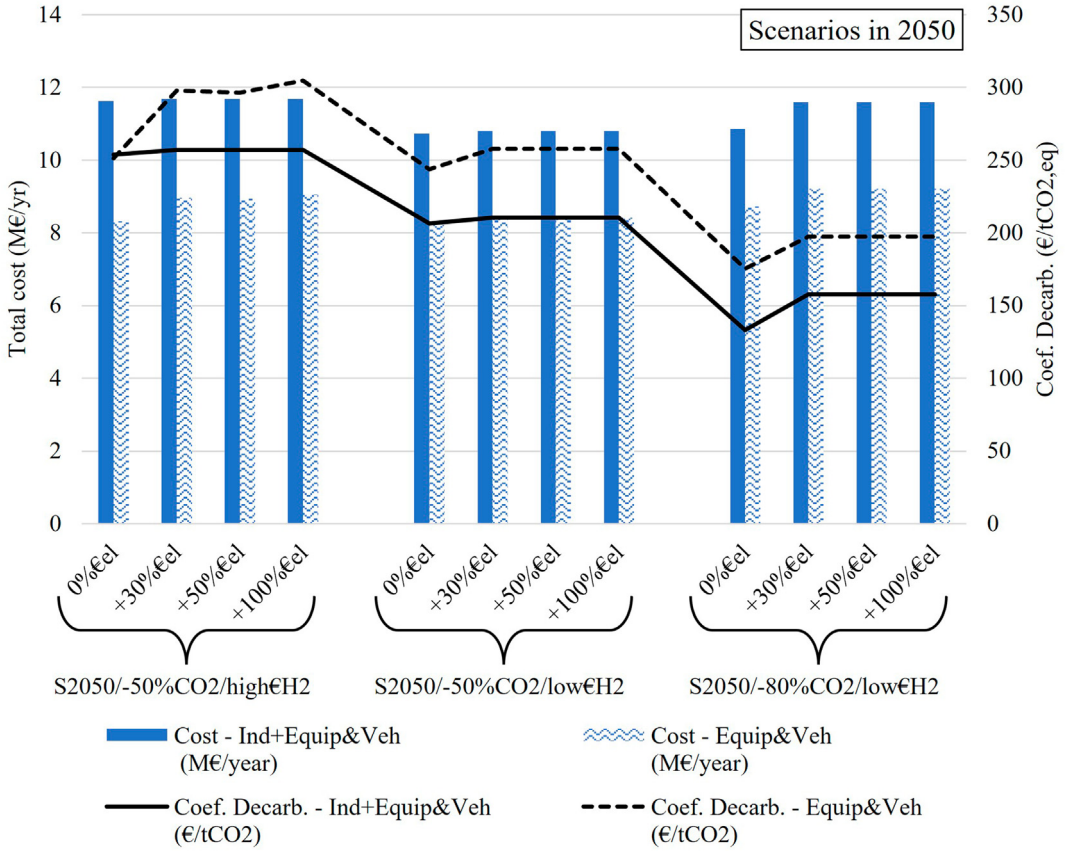

Fig. 10 – Total costs of the system (bars, left axis) and the related decarbonization coefficient (lines, right axis) of the two energy system substructures with and without industry in 2050. Solid bars and lines refer to the substructure with the industry ("Ind + Equip&Veh"), while wave bars and dashed lines to the substructure without industry ("Equip&Veh").

same emission reduction target, the replacement of port equipment and vehicles is more expensive than the replacement of H_2 as feedstock for the industry. In fact, the replacement of equipment and vehicles requires a remarkable initial investment effort to purchase new equipment and vehicles and associated infrastructures (e.g., refuelling/charging stations). Conversely, this is not necessary in the case of replacing H_2 for the industry. This result suggests that it is more cost-effective to undertake decarbonization strategies if the port is located in the vicinity of an industrial hub.

In both Figs. 9 and 10, within each scenario, the decarbonization coefficient of the "*Equip&Veh*" substructure (dashed black line) increases as the cost of the battery electric equipment and vehicles increases, whereas the same coefficient for the "*Ind + Equip&Veh*" substructure (solid black line) remains almost constant except for the *S2050/-80%CO2/low€H2* scenario. This result is another consequence of the reduced dependency of the decarbonization of the substructure with industry on the replacement cost of electric equipment and vehicles. Only in the *S2050/-80%CO2/low€H2* scenario, the decarbonization coefficient of the "*Ind + Equip&Veh*" substructure increases. This different trend can be explained by the fact that the decarbonization of the equipment and vehicle fleet is necessary in this scenario to achieve the required environmental target, in addition to the replacement of the grey H_2 supplied to the industry.

As shown in Figs. 9 and 10, decarbonization coefficients in 2050 are about two to three times lower than in 2030, due to lower estimated costs for new technologies and green energy sources. In particular, NH_3 imported in 2050 at lower price (*low€H2*) allows a marked reduction of costs for the decarbonization of the IPA superstructure, both with and without the industry H_2 demand.

Conclusions

This paper evaluates different configurations of energy conversion and storage systems in an industrial port area (IPA) to select the most cost-effective ones for different target levels of $CO_{2,eq}$ emissions.

These configurations are part of a complete superstructure including renewable and fossil energy sources, the import or local production of hydrogen, the supply of hydrogen to a nearby steel industry, equipment/vehicles powered by Diesel, electricity or hydrogen along with the refuelling and storage stations/units. A Mixed Integer Linear Programming (MILP) design-operation optimization problem is set up based on one-year operation of the IPA. The optimization is carried out by considering two substructures within the superstructure, one including the energy demands of both industry and port vehicles/equipment, the other only the energy demand of port

equipment/vehicles. For each substructure, different optimization runs are performed for the years 2030 and 2050. Specific emission reduction targets and different scenarios of costs of energy conversion and storage units, infrastructures, and imported hydrogen are considered, as well.

The outcomes of the optimization prove that:

- Electrification and hybridization are crucial for decarbonizing the IPA in the medium-to-long term. Hybrid Diesel are mainly used to reduce the carbon footprint of the port by 30%–50%. Hybrid diesel vehicles give way to battery electric and hybrid hydrogen vehicles if more stringent emission targets (i.e., 50–80%) are imposed, especially when the steel industry emissions are disregarded from the analysis. In 2050, when 50% and 80% emission reduction is required, the optimization of both substructures suggests including hydrogen vehicles supplied by both grey and green hydrogen (either locally produced or imported) when the price of battery electric vehicles is higher than the projected one in 2050 (from 30% and up).
- Ammonia plays a key role for decarbonizing industry and heavy-duty vehicles in the 2050 cost/emissions scenarios, when the cost of extracted hydrogen from ammonia is expected to be 2.25 €/kg_{H2}. With emission reduction targets of 80% and 50%, imported ammonia meets most and some of the vehicles and industry demands, respectively. When costs exceeds 2.25 €/kg_{H2}, as in 2030, the IPA can only achieve a −30% emission reduction by converting vehicles to hybrid Diesel and battery electric ones, and/or using locally available renewable energy sources to produce hydrogen for the industry.
- The cost for avoiding CO_2 emissions is always higher for the substructure without the industry. Thus, achieving the same emission reduction goal is more expensive by replacing port vehicles than by substituting hydrogen as a feedstock for industry. In fact, the replacement of vehicles implies the purchase of all associated equipment such as vehicles and refuelling stations that are not necessary in the case of replacing hydrogen for the industry.

Although there are several sources of uncertainty that may affect the optimization results, this study can provide valuable insights into technologies and strategies that can be implemented not only in the IPA under consideration but also in other industrial complexes or areas where heavy-duty vehicles operate and there is industrial demand of hydrogen.

A sensitivity analysis of other input parameters, e.g., different locations of the IPA, types of energy demand within the IPA, future financial support tools, which substantially influence optimization results and the choice of one strategy over others, could be the focus of further works.

Declaration of competing interest

The authors declare that they have no known competing financial interests or personal relationships that could have appeared to influence the work reported in this paper.

Acknowledgments

D.P., C.D. and R.T. acknowledge the financial support from the project sHYpS (sustainable HYdrogen powered Shipping, Horizon Europe call Horizon-CL5-2021-D5-01).

Appendix A. Supplementary data

Supplementary data to this article can be found online at https://doi.org/10.1016/j.ijhydene.2023.07.008.

REFERENCES

[1] EU Action n.d. https://ec.europa.eu/clima/eu-action_en (accessed March 16, 2022).
[2] United Nations Conference on Trade and Development (Unctad). Review of maritime transport. n.d.https://unctad.org/publication/review-maritime-transport-2022 (accessed March 15, 2022)
[3] Merk O. The Competitiveness of global port-Cities. OECD READ edition; 2010. p. 184.
[4] Rødseth KL, Schøyen H, Wangsness PB. Decomposing growth in Norwegian seaport container throughput and associated air pollution. Transp Res Part D Transp Environ 2020;85:102391. https://doi.org/10.1016/J.TRD.2020.102391.
[5] Griffiths S, Sovacool BK, Kim J, Bazilian M, Uratani JM. Industrial decarbonization via hydrogen: a critical and systematic review of developments, socio-technical systems and policy options. Energy Res Soc Sci 2021;80:102208. https://doi.org/10.1016/J.ERSS.2021.102208.
[6] SUstainable Ports in the Adriatic-Ionian Region (SUPAIR) n.d. https://supair.adrioninterreg.eu/(accessed March 16, 2022).
[7] Sciberras EA, Zahawi B, Atkinson DJ, Juandó A, Sarasquete A. Cold ironing and onshore generation for airborne emission reductions in ports. https://doi.org/10.1177/1475090214532451; 2014. https://doi.org/10.1177/1475090214532451.
[8] Transboundary Waters Assessment Programme (TWAP) — GEF TWAP n.d. http://geftwap.org/twap-project (accessed March 16, 2022).
[9] Iris Ç, Lam JSL. A review of energy efficiency in ports: operational strategies, technologies and energy management systems. Renew Sustain Energy Rev 2019;112:170–82. https://doi.org/10.1016/J.RSER.2019.04.069.
[10] Sifakis N, Tsoutsos T. Planning zero-emissions ports through the nearly zero energy port concept. J Clean Prod 2021;286:125448. https://doi.org/10.1016/J.JCLEPRO.2020.125448.
[11] Cunanan C, Tran MK, Lee Y, Kwok S, Leung V, Fowler M. A review of heavy-duty vehicle powertrain technologies: diesel engine vehicles, battery electric vehicles, and hydrogen fuel cell electric vehicles. Clean Technol 2021;3:474–89. https://doi.org/10.3390/CLEANTECHNOL3020028. 2021;3:474–89.
[12] Kim J, Rahimi M, Newell J. Http://DxDoiOrg/101080/155683182011606353. Life-cycle emissions from port electrification: a case study of cargo handling tractors at the port of Los Angeles, vol. 6; 2011. p. 321. https://doi.org/10.1080/15568318.2011.606353. 37.
[13] Wei HL, Gu W, Chu JX. The dynamic power control technology for the high power Lithium battery hybrid

rubber-tired gantry (RTG) crane. IEEE Trans Ind Electron 2019;66:132–40. https://doi.org/10.1109/TIE.2018.2816011.
[14] Di Ilio G, Di Giorgio P, Tribioli L, Bella G, Jannelli E. Preliminary design of a fuel cell/battery hybrid powertrain for a heavy-duty yard truck for port logistics. Energy Convers Manag 2021;243:114423. https://doi.org/10.1016/J.ENCONMAN.2021.114423.
[15] Densberger NL, Bachkar K. Towards accelerating the adoption of zero emissions cargo handling technologies in California ports: Lessons learned from the case of the Ports of Los Angeles and Long Beach. J Clean Prod 2022;347:131255. https://doi.org/10.1016/J.JCLEPRO.2022.131255.
[16] Ahamad NB, Othman M, Vasquez JC, Guerrero JM, Su CL. Optimal sizing and performance evaluation of a renewable energy based microgrid in future seaports. Proc IEEE Int Conf Ind Technol 2018;2018. https://doi.org/10.1109/ICIT.2018.8352322. February:1043–8.
[17] Wang W, Peng Y, Li X, Qi Q, Feng P, Zhang Y. A two-stage framework for the optimal design of a hybrid renewable energy system for port application. Ocean Eng 2019;191:106555. https://doi.org/10.1016/J.OCEANENG.2019.106555.
[18] Prousalidis J, Antonopoulos G, Patsios C, Greig A, Bucknall R. Green shipping in emission controlled areas: Combining smart grids and cold ironing. Proc - 2014 Int Conf Electr Mach ICEM 2014 2014:2299. https://doi.org/10.1109/ICELMACH.2014.6960506. 305.
[19] Geerlings H, Heij R, van Duin R. Opportunities for peak shaving the energy demand of ship-to-shore quay cranes at container terminals. J Shipp Trade 2018 31 2018;3:1–20. https://doi.org/10.1186/S41072-018-0029-Y.
[20] Kinnon M Mac, Razeghi G, Samuelsen S. The role of fuel cells in port microgrids to support sustainable goods movement. Renew Sustain Energy Rev 2021;147:111226. https://doi.org/10.1016/J.RSER.2021.111226.
[21] van Biert L, Godjevac M, Visser K, Aravind PV. A review of fuel cell systems for maritime applications. J Power Sources 2016;327:345–64. https://doi.org/10.1016/J.JPOWSOUR.2016.07.007.
[22] Dall'Armi C, Pivetta D, Taccani R. Hybrid PEM fuel cell power plants fuelled by hydrogen for improving Sustainability in shipping: state of the Art and review on active Projects. Energies 2023;16:2022. https://doi.org/10.3390/EN16042022/S1.
[23] Pivetta D, Dall'Armi C, Taccani R. Multi-objective optimization of hybrid PEMFC/Li-ion battery propulsion systems for small and medium size ferries. Int J Hydrogen Energy 2021;46:35949–60. https://doi.org/10.1016/J.IJHYDENE.2021.02.124.
[24] sHYpS: Sustainable HYdrogen powered Shipping, https://www.shyps.eu/
[25] Petkov I, Gabrielli P. Power-to-hydrogen as seasonal energy storage: an uncertainty analysis for optimal design of low-carbon multi-energy systems. Appl Energy 2020;274:115197. https://doi.org/10.1016/J.APENERGY.2020.115197.
[26] Sustainable Ports as Energy Hubs n.d. https://www.maritime-executive.com/editorials/sustainable-ports-as-energy-hubs (accessed March 16, 2022).
[27] Mallouppas G, Ioannou C, Yfantis EA. A review of the latest trends in the Use of green ammonia as an energy carrier in maritime industry. Energies 2022;15:1453. https://doi.org/10.3390/EN15041453. 2022;15:1453.
[28] IRENA (International Renewable Energy Agency). Global hydrogen trade to meet the 1.5°C Climate goal: (Part I) trade Outlook for 2050 and way forward. 2022.
[29] IRENA (International Renewable Energy Agency). Global hydrogen trade to meet the 1.5°C Climate goal: (Part II) technology review of hydrogen carriers. In: Glob Hydrog trade to meet 15°C Clim goal Technol Rev Hydrog carriers; 2022.
[30] sustainable HYdrogen powered Shipping (sHYpS) project, n.d. https://cordis.europa.eu/project/id/101056940 (accessed July 20, 2023).
[31] Williamsson J, Costa N, Santén V, Rogerson S. Barriers and Drivers to the implementation of Onshore power supply—a literature review. Sustain Times 2022;14:6072.
[32] J2601: Fueling Protocols for Light Duty Gaseous Hydrogen Surface Vehicles - SAE International n.d. https://www.sae.org/standards/content/j2601_201407/(accessed March 15, 2022).
[33] Minutillo M, Perna A, Forcina A, Di Micco S, Jannelli E. Analyzing the levelized cost of hydrogen in refueling stations with on-site hydrogen production via water electrolysis in the Italian scenario. Int J Hydrogen Energy 2021;46:13667–77. https://doi.org/10.1016/J.IJHYDENE.2020.11.110.
[34] Hurskainen M. Industrial oxygen demand in Finland. 2017. n.d. https://cris.vtt.fi/en/publications/industrial-oxygen-demand-in-finland (accessed March 15, 2022).
[35] ElectricityMap n.d. https://app.electricitymap.org/(accessed March 15, 2022).
[36] BrainBlog Energy. In: EU Energy Outlook 2050: How will the European electricity market develop over the next 30 years?; 2022. https://blog.energybrainpool.com/en/eu-energy-outlook-2050-how-will-the-european-electricity-market-develop-over-the-next-30-years/ (accessed March 9, 2023).
[37] Renquist JV, Dickman B, Bradley TH. Economic comparison of fuel cell powered forklifts to battery powered forklifts. Int J Hydrogen Energy 2012;37:12054–9. https://doi.org/10.1016/J.IJHYDENE.2012.06.070.
[38] U.S. Department of Energy. Chapter five: Infrastructure n.d. https://www.energy.gov/sites/default/files/2022-10/Chapter_5-Infrastructure.pdf (accessed March 26, 2023).
[39] Kim J, Sovacool BK, Bazilian M, Griffiths S, Lee J, Yang M, et al. Decarbonizing the iron and steel industry: a systematic review of sociotechnical systems, technological innovations, and policy options. Energy Res Soc Sci 2022;89:102565. https://doi.org/10.1016/J.ERSS.2022.102565.
[40] International Energy Agency (IEA) - The Future of Hydrogen n.d. https://www.iea.org/reports/the-future-of-hydrogen (accessed March 16, 2022)..
[41] Vogl V, Åhman M, Nilsson LJ. Assessment of hydrogen direct reduction for fossil-free steelmaking. J Clean Prod 2018;203:736–45. https://doi.org/10.1016/J.JCLEPRO.2018.08.279.
[42] Fossil free steel - SSAB n.d. https://www.ssab.com/en/fossil-free-steel (accessed March 9, 2023).
[43] Graf M, Holm T, Wiberg S. Neutral hardening and annealing. Furn Atmos No2 2017:33–56.
[44] Pivetta D, Dall'Armi C, Taccani R. Multi-objective optimization of a hydrogen hub for the decarbonization of a port industrial area. J Mar Sci Eng 2022;10:231. https://doi.org/10.3390/JMSE10020231. 2022;10:231.
[45] Useable battery capacity of full electric vehicles cheatsheet - EV Database n.d. https://ev-database.org/cheatsheet/useable-battery-capacity-electric-car (accessed March 14, 2023)..
[46] Electric forklift battery Program Expanding to 25 models by 2020 n.d. https://essexfurukawa.com/news/electrovayas-electric-forklift-battery-line-expanded-to-more-than-25-models/ (accessed March 14, 2023).
[47] E-Rtg - Cavotec Sa n.d. www.cavotec.com/en/your-applications/ports-maritime/crane-electrification/e-rtg (accessed March 14, 2023).
[48] Electric Tractor Units Are in Trouble. Where Is The Way Out? | by Moneyball | Medium n.d. https://moneyballr.medium.

com/electric-tractor-units-are-in-trouble-where-is-the-way-out-eb34000dc575 (accessed March 14, 2023)..
[49] Kalmar Global n.d. https://www.kalmarglobal.com/(accessed March 15, 2022).
[50] XCMG - 45 ton electric reach stacker for container-Reach Stacker-Xuzhou Unique Construction Machinery Co.,Ltd n.d. http://www.craneunique.com/chanpin_61/781.html (accessed March 14, 2023).
[51] Edge JS, O'Kane S, Prosser R, Kirkaldy ND, Patel AN, Hales A, et al. Lithium ion battery degradation: what you need to know. Phys Chem Chem Phys 2021;23:8200–21. https://doi.org/10.1039/D1CP00359C.
[52] EV Charging | Electric Vehicle Chargers | ABB n.d. https://new.abb.com/ev-charging/(accessed March 15, 2022).
[53] JuicePump 75 and Flexi 150 - EV Commercial Fast Charging Station | Enel X n.d. https://evcharging.enelx.com/eu/commercial/juicepump75-and-flexi150 (accessed March 15, 2022).
[54] Nicholas M. Estimating electric vehicle charging infrastructure costs across major U.S. metropolitan areas. 2019.
[55] Haskel High Pressure Technology - Hydrogen Solutions n.d. https://www.haskel.com/en-us (accessed March 15, 2022).
[56] Hydrogen refueling technologies - Linde Engineering https://www.linde-engineering.com/en/plant-components/hydrogen-refueling-technologies/index.html (accessed March 15, 2022).
[57] Perna A, Minutillo M, Di Micco S, Jannelli E. Design and costs analysis of hydrogen refuelling stations based on different hydrogen sources and plant configurations. Energies 2022;15:541. https://doi.org/10.3390/EN15020541. 2022;15:541.
[58] International Energy Agency (IEA). World energy Outlook. 2022. n.d. https://www.iea.org/reports/world-energy-outlook-2022 (accessed March 15, 2022).
[59] Klanšek U. A comparison between MILP and MINLP approaches to optimal solution of Nonlinear Discrete Transportation Problem. Vilnius Gedim Tech Univ 2015;30:135–44. https://doi.org/10.3846/16484142.2014.933361.
[60] Rech S. Smart energy systems: Guidelines for modelling and optimizing a fleet of Units of different configurations. Energies 2019;12:1320. https://doi.org/10.3390/EN12071320. 2019;12:1320.
[61] Ito K, Yokoyama R, Akagi S, Yamaguchi T, Matsumoto Y. Optimal operational Planning of a gas turbine combined heat and power plant based on the Mixed-integer programming. IFAC Proc 1988;21:371–7. https://doi.org/10.1016/S1474-6670(17)53769-6.
[62] Consonni S, Lozza G, Macchi E. Optimization of Cogeneration systems operation—Part B: solution Algorithm and examples of optimum operating strategies. In: ASME int. Symp. Turbomachinery, Comb. Technol. Cogener.; 1989. Nice, France.
[63] Rech S. Analisi e ottimizzazione della configurazione di un macrosistema di conversione di energia. Università degli studi di Padova; 2013.
[64] Dall'Armi C, Pivetta D, Taccani R. Uncertainty analysis of the optimal health-conscious operation of a hybrid PEMFC coastal ferry. Int J Hydrogen Energy 2022;47:11428–40. https://doi.org/10.1016/J.IJHYDENE.2021.10.271.
[65] Gabrielli P, Gazzani M, Martelli E, Mazzotti M. Optimal design of multi-energy systems with seasonal storage. Appl Energy 2018;219:408–24. https://doi.org/10.1016/J.APENERGY.2017.07.142.
[66] Python.org website n.d. https://www.python.org/ (accessed May 22, 2023).
[67] Gurobi Optimization website n.d. https://www.gurobi.com/ (accessed March 15, 2022).
[68] JRC Photovoltaic Geographical Information System (PVGIS) - European Commission n.d. https://re.jrc.ec.europa.eu/pvg_tools/en/ (accessed March 15, 2022).
[69] Riaz A, Sarker MR, Saad MHM, Mohamed R. Review on comparison of different energy storage technologies used in Micro-energy Harvesting, WSNs, low-cost Microelectronic Devices: Challenges and Recommendations. Sensors 2021;21:5041. https://doi.org/10.3390/S21155041. 2021;21:5041.
[70] Viktorsson L, Heinonen JT, Skulason JB, Unnthorsson R. A step towards the hydrogen Economy—a life cycle cost analysis of A hydrogen refueling station. Energies 2017;10:763. https://doi.org/10.3390/EN10060763. 2017;10:763.